



Determinants of L-band backscatter in dry tropical ecosystems: Implications for biomass mapping

João M.B. Carreiras ^{a,b,c,*}, Thomas Higginbottom ^{c,d}, John L. Godlee ^{c,e}, Sam Harrison ^c, Lorena Benitez ^c, Penelope J. Mograbi ^{b,c,e,f}, Aurora Levesley ^g, Karina Melgaço ^g, David Milodowski ^{b,c}, Georgia Pickavance ^g, Geoff Wells ^c, Edmar Almeida de Oliveira ^h, Luzmila Arroyo ⁱ, Sam Bowers ^c, Roel J.W. Brienen ^g, Domingos Cardoso ^j, António Alberto Jorge Farias Castro ^k, Ezequiel Chavez ⁱ, Ítalo A.C. Coutinho ^l, Tomás F. Domingues ^m, Fernando Elias ⁿ, Mário Marcos Espírito Santo ^o, Ted R. Feldpausch ^p, David Galbraith ^g, Emanuel Gloor ^g, Francisco M.P. Gonçalves ^{e,q,r,s}, Tatenda Gotore ^{e,f}, Francoise Yoko Ishida ^t, Timothy J. Killeen ^u, Yadvinder Malhi ^v, Beatriz S. Marimon ^h, Ben Hur Marimon-Júnior ^h, Desirée Marques Ramos ^w, Simone Matias de Almeida Reis ^{h,x}, Ian McNicol ^c, Edward T.A. Mitchard ^y, Peter Moonlight ^z, Paulo S. Morandi ^h, Patricia Morellato ^w, Anderson Muchawona ^{e,aa}, Jonathan Muledi ^{e,ab}, Alejandro Murakami ⁱ, Mylor Ngoy Shutcha ^{ab}, Paula Nieto-Quintano ^y, Alexander Parada-Gutierrez ⁱ, Nayane Cristina Candida dos Santos Prestes ^h, Luciano Paganucci de Queiroz ^{ac}, Priscyla M.S. Rodrigues ^{ad}, Jhonathan Oliveira Silva ^{ad}, Rubens M. Santos ^{ae}, Tiina Särkinen ^{af}, Domingos Fortunato P.F. Silva ^q, Tony C. de Sousa Oliveira ^m, Marc Steininger ^{ag}, José Tchamba ^q, Elmar Veenendaal ^{ah}, Débora Zuanny ^{af}, Tim R. Baker ^g, Kyle G. Dexter ^{c,e}, Gabriele Hegerl ^c, R. Toby Pennington ^{p,af}, Oliver L. Phillips ^g, Stephen Sitch ^p, Mathew Williams ^{b,c}, Shaun Quegan ^{a,b}, Casey M. Ryan ^{b,c,e}

^a School of Mathematics and Statistics, University of Sheffield, Sheffield, United Kingdom

^b National Centre for Earth Observation, Leicester, United Kingdom

^c School of GeoSciences, University of Edinburgh, Edinburgh, United Kingdom

^d Airbus Defence and Space, Surrey Research Park, Guildford, United Kingdom

^e Socio-Ecological Observatory for Studying African Woodlands (SEOSAW), South Africa

^f School of Animal, Plant and Environmental Sciences, University of the Witwatersrand, Wits, South Africa

^g School of Geography, University of Leeds, Leeds, United Kingdom

^h Programa de Pós-Graduação em Ecologia e Conservação, Universidade do Estado de Mato Grosso, Nova Xavantina, Mato Grosso, Brazil

ⁱ Museo de Historia Natural Noel Kempff Mercado, Universidad Autónoma Gabriel Rene Moreno, Santa Cruz, Bolivia

^j Instituto de Pesquisas Jardim Botânico do Rio de Janeiro, Rio de Janeiro, Brazil

^k Departamento de Biología, Programa BIOTEN, Universidade Federal do Piau, Teresina, Piau, Brazil

^l Centro de Ciências, Departamento de Biología, Universidade Federal do Ceará, Programa de Pós-Graduação em Sistemática, Uso e Conservação da Biodiversidade, Fortaleza, Ceará, Brazil

^m Departamento de Biología, Faculdade de Filosofia, Ciências e Letras de Ribeirão Preto, Universidade de São Paulo, Ribeirão Preto, São Paulo, Brazil

ⁿ Embrapa Amazônia Oriental, Belém, Pará, Brazil

^o Departamento de Biología Geral, Universidade Estadual de Montes Claros, Montes Claros, Minas Gerais, Brazil

^p Geography, Faculty of Environment, Science and Economy, University of Exeter, Exeter, United Kingdom

^q Centro de Estudos da Biodiversidade e Educação Ambiental, Instituto Superior de Ciências da Educação da Huila, Lubango, Huila, Angola

^r Universidade Mandume Ya Ndemufayo, Lubango, Angola

* Corresponding author at: School of GeoSciences, University of Edinburgh, Edinburgh, United Kingdom

E-mail address: v1jcarr8@ed.ac.uk (J.M.B. Carreiras).

^s cE3c - Center for Ecology, Evolution and Environmental Changes, Faculdade de Ciências da Universidade de Lisboa, Lisboa, Portugal

^t Centre for Tropical Environmental and Sustainability Science, College of Science and Engineering, James Cook University, Australia

^u Agteca-Amazonica, Santa Cruz, Bolivia

^v Environmental Change Institute, School of Geography and the Environment, University of Oxford, Oxford, United Kingdom

^w Center for Research on Biodiversity Dynamics and Climate Change and Department of Biodiversity, Phenology Lab, UNESP - São Paulo State University, Biosciences

Institute, São Paulo, Rio Claro, Brazil

^x Centro de Ciências Biológicas e da Natureza, Universidade Federal do Acre, Rio Branco, Acre, Brazil

^y Space Intelligence, Edinburgh, United Kingdom

^z Botany, School of Natural Sciences, Trinity College Dublin, Dublin 2, Ireland

^{aa} Zimbabwe Forestry Commission, Harare, Zimbabwe

^{ab} Ecologie, Restauration Ecologique et Paysage, Faculté des Sciences Agronomiques, Université de Lubumbashi, the Democratic Republic of the Congo

^{ac} Departamento de Ciências Biológicas, Universidade Estadual de Feira de Santana, Feira de Santana, Bahia, Brazil

^{ad} Colegiado de Ecología, Universidade Federal do Vale do São Francisco, Senhor do Bonfim, Bahia, Brazil

^{ae} Departamento de Ciencias Florestais, Universidade Federal de Lavras, Lavras, Minas Gerais, Brazil

^{af} Royal Botanic Garden Edinburgh, United Kingdom

^{ag} Conservation International, United States of America

^{ah} Plant Ecology and Nature Conservation Group, Wageningen University, Wageningen, the Netherlands

ARTICLE INFO

Edited by Jing M. Chen

Keywords:

Dry tropics

Forests

Savannas

Stem biomass

Stem density

Aboveground biomass density

Soil properties

L-band synthetic aperture radar (SAR)

Polarimetric decomposition

Structural equation modelling

ABSTRACT

Accurate characterization of the role of the dry tropics in the global carbon cycle requires precise estimation of woody biomass changes due to ecological and anthropogenic change, including deforestation, forest degradation, regrowth, mortality and enhanced tree growth due to climate change. L-band Synthetic Aperture Radar (SAR) backscatter observations offer a reliable option to consistently map these processes as they are (i) available globally since 2007 (JAXA ALOS-1, ALOS-2 and ALOS-4), and (ii) sensitive to woody structure, such as above-ground biomass density (*AGBD*) up to $\sim 100 \text{ t ha}^{-1}$. However, we lack multi-site empirical understanding of the scattering processes that determine the relationship between L-band SAR and woody vegetation structure in the dry tropics, and how this is mediated by soil properties.

This study used observations from ground plots in Africa ($n = 171$), Australia ($n = 6$), and South America ($n = 44$) to understand the impact of vegetation structure and soil properties on spatially and temporally coincident fully-polarimetric L-band SAR data. Fully-polarimetric L-band SAR single-look complex data were converted to scattering mechanisms/parameters using van Zyl, Cloude-Pottier, and Freeman-Durden polarimetric decompositions to elucidate the physical mechanisms involved. Multivariate SAR-vegetation-soil relationships were analysed using a theory-informed structural equation modelling approach. The strongest positive effects on volume scattering come from stem density (stems ha^{-1}) and mean stem biomass of trees, and soil water and sand content (standardized regression coefficients of 0.3, 0.1, 0.2 and 0.1, respectively). The only significant effect on surface scattering is from stem density (0.1). Significant effects on double bounce scattering are from stem density (0.3) and soil sand content (-0.2). Since *AGBD* is the product of stem density and mean stem biomass, this modelling framework points to a stronger effect from the number of trees rather than their size/biomass. Therefore, *AGBD* maps relying solely on radar intensity may not reflect significant changes when *AGBD* is increasing due to the growth of existing stems. Additionally, such maps might overestimate changes in *AGBD* when driven by the recruitment of new stems or loss of existing stems. Full-polarimetric observations allow the decomposition of the radar signal into volume scattering, surface scattering, and double bounce, enabling the inversion of structural equation models to retrieve both stem density and mean stem biomass. This provides a more comprehensive description of forest structure compared to retrieving only *AGBD*. As this approach depends on full-polarimetric data, its effectiveness is closely tied to the availability of such observations. Our findings underscore the value of recent and upcoming missions such as ALOS-4 PALSAR-3, BIOMASS and ROSE-L, and highlight the need to prioritise the acquisition of quad-pol SAR data to support future large-scale retrieval of vegetation structure attributes.

1. Introduction

The dry tropics encompass complex and heterogeneous vegetation structures, from open savannas to closed canopy woodlands and dry forests and extend across ~ 15 million km^2 (Pennington et al., 2018). These vegetation types are extremely important land systems in terms of carbon cycling (Piao et al., 2020), biodiversity (DRYFLOR et al., 2016) and are key to the livelihoods of hundreds of millions of people (Djoudi et al., 2015). Models suggest that the global dry tropics are the largest, most climate-sensitive, and fastest increasing component of the land carbon sink (Ahlstrom et al., 2015). However, there is high uncertainty about the carbon fluxes from land processes in these regions (Arneth et al., 2017), and a more accurate understanding of the structure of vegetation and its dynamics in the dry tropics is essential. For example, much improved estimates of aboveground biomass density (*AGBD*) dynamics from land-use and land cover change in the dry tropics are vital to better constrain the geographic distribution of the land carbon sink and its recent trends, and to support action to protect and explore the

potential for carbon sequestration in these lands (Piao et al., 2018).

Accurate characterization of the role of the dry tropics in the global carbon cycle requires precise and unbiased estimation of *AGBD* and its dynamics due to natural and anthropogenic causes, e.g., deforestation, forest degradation, mortality, regrowth and tree growth. L-band Synthetic Aperture Radar (SAR) observations are currently being used to consistently map these dynamics (McNicol et al., 2023; McNicol et al., 2018). Furthermore, L-band SAR observations are well suited to mapping forest structure in the dry tropics, where *AGBD* rarely exceeds 100 t ha^{-1} (Gou et al., 2022; Rodriguez-Veiga et al., 2020; Ryan et al., 2012; Ryan et al., 2011; Urbazaev et al., 2015; Wessels et al., 2023). However, a lack of representative ground observations and limited understanding of the interaction between radar observations and vegetation and soil characteristics in these lower biomass systems have generally resulted in biased and imprecise *AGBD* estimates (Araza et al., 2022). It is therefore critical to have an accurate understanding of how vegetation structure and soil characteristics affect the signal measured by L-band SAR sensors.

Although local studies based on airborne sensors have been fundamental in investigating the relationships between biomass, frequency and polarisation (Le Toan et al., 1992) and the particular value of L-band compared to P-band in lower biomass forests (Lucas et al., 2006; Schlund and Davidson, 2018; Tanase et al., 2014), the emphasis changed to large scale applications with the advent of spaceborne L-band data. Dual- and fully-polarimetric L-band observations have been available globally since 2007 from the Japanese Aerospace Exploration Agency (JAXA) Advanced Land Observing Satellite (ALOS) Phased Array L-band SAR (PALSAR) sensors (ALOS-1 PALSAR-1: 2006–2011, ALOS-2 PALSAR-2: 2014–present, ALOS-4 PALSAR-3: launched in 2024, and also from the SAOCOM mission since 2018 (Palomeque et al., 2024). Fully polarimetric SAR systems transmit and receive the electric field in horizontal and vertical polarisations, with the resulting scattering matrix containing the complete information about the characteristics of the scatterers (i.e., the observed objects on the ground) (Lee and Pottier, 2009). For distributed scatterers, such as woody vegetation, the information is contained in the covariance or coherency matrices, which describe the average backscatter properties of a region or window of interest. These matrices can be decomposed into three scattering mechanism that are thought to be dominant over land surfaces: surface scattering, volume scattering and double bounce. Their relative importance depends on i) the structure of the scatterers (e.g., the shape, size, and orientation of tree branches), ii) soil roughness and texture, and iii) dielectric properties of the scatterers (essentially, their water content) (Cloude and Pottier, 1996).

Methods to extract information about the scattering mechanisms from fully-polarimetric SAR data over land surfaces can be divided into two types: those relying on the eigenvalue/eigenvector decomposition of the covariance or coherency matrices (Cloude, 1985; Cloude and Pottier, 1997; van Zyl, 1993) or model-based approximations to the scattering problem (Freeman and Durden, 1998; Yamaguchi et al., 2005). Eigenvalue/eigenvector decomposition focuses on the statistical properties and dimensionality reduction of SAR data, while model-based decompositions aim to characterise the scattering mechanisms and polarisation properties of the targets. In this study, we assess the information content provided by both methods and how they relate to vegetation structure and soil properties.

The magnitude and relative importance of each scattering mechanism is also affected by characteristics of the sensor, such as frequency and incidence angle (Le Toan et al., 1992). Most studies using fully polarimetric spaceborne L-band SAR data to retrieve vegetation structure were carried out at local level and in boreal (Antropov et al., 2017; Chowdhury et al., 2014) or moist forests (Bharadwaj et al., 2015; Cassol et al., 2019; Wiederkehr et al., 2020). In vegetation, the shape, size and orientation of the main scatterers (which may be the leaves, twigs, branches or trunks, depending on the wavelength) can affect the return at each polarisation (Tanase et al., 2013). In the dry tropics, soil and vegetation characteristics exhibit distinct ecological and physical properties compared to temperate and moist forest systems. Firstly, soil moisture content tends to be lower due to seasonal precipitation and higher evapotranspiration rates, leading to drier soils. This results in a higher proportion of bare ground and lower woody vegetation density, impacting the scattering mechanisms observed by SAR sensors. Additionally, vegetation in the dry tropics often comprises sparse, shorter woody vegetation with smaller leaf sizes and lower AGBD than the denser, taller vegetation found in temperate and moist forests. These differences in vegetation structure affect the scattering behaviour of radar signals, with sparse canopies exhibiting stronger surface scattering and reduced volume scattering compared to denser canopies. Furthermore, the prevalence of woody vegetation with complex (e.g. multi stemmed, non-vertical and “umbrella” shaped) branch architectures in the dry tropics introduces additional complexities in radar signal interactions.

Several studies have highlighted the impact of AGBD and soil properties on the signal measured by L-band SAR sensors (Gou et al., 2022;

Lucas et al., 2010; Wessels et al., 2023; Williams et al., 2022; Yu and Saatchi, 2016). Surface roughness and soil moisture are the main factors affecting scattering from the soil, both directly and via the double bounce mechanism. Surface scatter decreases as incidence angle increases but increases with increasing dielectric constant (Richards, 2009). Also important is surface slope, which affects surface and double bounce scattering. The dielectric constant of the scatterers within the vegetation, which is strongly correlated with moisture content, has large effects on the strength of scattering and attenuation by the canopy and hence on the strength of the return from surface scattering.

Much less attention has been given to understanding the contribution of woody vegetation structure to backscatter. Most studies are based almost entirely on scattering models (e.g. (Brolly and Woodhouse, 2012)) or relying on scattering models together with limited ground observations (Mermoz et al., 2015; Smith-Jonforsen et al., 2007). Using microwave modelling and P-band data from boreal forests, Smith-Jonforsen et al. (2007) found very large dispersion in the relationship between HV backscattering coefficient and AGBD, essentially depending on stand structure (i.e., few large vs many small trees). However, a much tighter relationship was found between HV backscatter and an indicator of stem biomass they termed the biomass-consolidation index. They concluded that information on stem density is needed to resolve ambiguities in estimation of AGBD from P-band SAR observations. Brolly and Woodhouse (2012) and Imhoff (1995) generalized this finding to other wavelengths. Brolly and Woodhouse (2012) used a simple one-layer microwave scattering model configured as a set of vertical cylinders parametrized by number (i.e., stem density) and average diameter to study their influence on VV-polarized SAR observations at P-band and VHF frequencies. They found a strong relationship between backscatter and AGBD only when stem density and average diameter were highly correlated with AGBD. However, these quantities can have different relationships with AGBD, depending on the type of vegetation: in some cases, AGBD is positively correlated with stem density and average diameter, whereas in others it is positively correlated with average diameter but negatively correlated with stem density. Brolly and Woodhouse (2012) and Woodhouse et al. (2012) concluded that backscatter does not respond to AGBD as such, but to structural properties that may be correlated with AGBD in different ways. However, this remains to be tested empirically at L-band.

There is therefore a need for an empirical understanding of how vegetation structure, particularly in the context of the dry tropics, influences the signal measured by L-band SAR sensors. This study therefore provides a large-scale analysis of the relationship between L-band microwave scattering mechanisms and woody vegetation structure and soil characteristics using L-band fully-polarimetric SAR data together with an extensive and representative set of ground observations acquired over the dry tropics. It aims to answer the following questions:

- 1) What are the dominant scattering mechanisms driving the L-band SAR signal in dry tropical savannas and woodlands?
- 2) What is the relative importance of vegetation structure and soil characteristics in controlling the L-band SAR signal from woody vegetation in the dry tropics?

2. Data and methods

2.1. Ground observations

Tree census data from permanent plots belonging to several networks were obtained over 12 locations across Africa, Australia and South America, with varying vegetation structures (Fig. 1, Supplementary Information Table S1, Supplementary Information Fig. S2).

The Socio-Ecological Observatory for Studying African Woodlands (SEOSAW: <https://seosaw.github.io/>) is a network of researchers making ground observations to study the ecological and human dimensions of African woodlands (The SEOSAW Partnership, 2021). This study uses

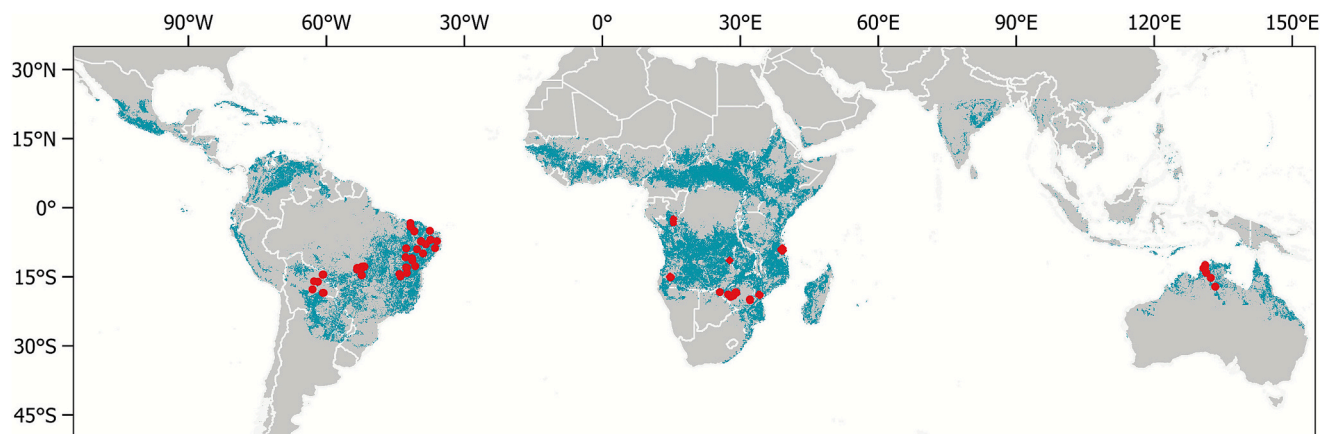


Fig. 1. Location of ground plots used as reference data (red dots). The 12 selected locations span the coverage of tropical dry forests and savannas (shown in cyan; Godlee et al. in prep). Angola/Bicuar, Congo/Lefini-Louna, DR Congo/Haut-Katanga, Mozambique/Gorongosa, Tanzania/Kilwa, Zimbabwe, Australia/Northern Territory, Brazil/Caatinga, Bolivia/Chiquitano, Bolivia/Huanchaca, Brazil/Nova Xavantina, Brazil/Roncador. (For interpretation of the references to colour in this figure legend, the reader is referred to the web version of this article.)

data from 171 permanent 1-ha plots in Bicuar National Park (Angola), Lefini Faunal Reserve and Louna Gorilla Sanctuary (Republic of the Congo), Haut-Katanga (Democratic Republic of the Congo), Gorongosa National Park (Mozambique), Kilwa district (Tanzania), and multiple districts of Zimbabwe.

In Australia, we used data from 6 1-ha plots in the Northern Territory (NTT) near Darwin, set up by Charles Darwin University and the Terrestrial Ecosystem Research Network (TERN). This dataset was obtained through Australia's TERN-Landscapes and Joint Remote Sensing Research Program (<https://field.jrsrp.com>).

Plot data in the dry tropics of South America were obtained through ForestPlots.net, a global partnership aimed at monitoring the world's tropical forests (ForestPlots.net et al., 2021; Lopez-Gonzalez et al., 2011). This study uses 29 permanent 1-ha plots collected in Chiquitano dry forests (Bolivia), Huanchaca (Bolivia), Nova Xavantina (Brazil), Serra do Roncador (Brazil), together with data from 15 0.5-ha plots in the Brazilian Caatinga (Moonlight et al., 2021).

The use of relatively large plots with 1 ha (except the 0.5 ha Caatinga plots) helps to minimise errors associated with geolocation and dilution bias, caused by heterogeneity at sub-hectare scales (Rejou-Mechain et al., 2014). Descriptors of woody vegetation structure at plot level were generated from stem-level measurements of diameter at breast height (DBH), height and wood density (inferred from species). AGBD (aboveground biomass density of all living stems per ha, in $t\ ha^{-1}$) was estimated by summing the biomass of each stem estimated from diameter measurements using the allometric equations of Chave et al. (2014); stem density (N , number of stems per ha) and mean stem biomass ($\bar{b} = AGBD/N$, in $t\ stem^{-1}$) were also estimated for all plots in this study. Table S1 (Supplementary Information) contains detailed information about the plots used, including the year the plots were measured. Only measurements of stems with DBH greater than 10 cm were used in the analysis to allow consistency between studies.

To relate the ground measurements to the SAR data, the vegetation descriptors obtained from a plot during a particular year were taken to represent the period covering two years on either side of that census (e.g., a census in 2005 represents the period from 2003 to 2007). When a plot had multiple censuses, annual estimates of the descriptors of vegetation structure between censuses were generated by linear interpolation.

2.2. L-band synthetic aperture radar (SAR) data

All available fully-polarimetric L-band SAR scenes acquired by ALOS-1 PALSAR-1 (2006–2011) and ALOS-2 PALSAR-2 (2014–present)

over the plot locations were downloaded and processed, yielding 59 acquisition dates in total, 18 for Africa, 9 for Australia and 32 for Latin America (Supplementary Information - Table S2 lists the scenes used). The polarimetric SAR data were downloaded in single-look complex (SLC) format, from which the local covariance and coherency matrices were calculated using a 5×5 window. The only difference between these two matrices is that the first is the covariance matrix arising from the measured complex signal, $(S_{hh}, \sqrt{2}S_{hv}, S_{vv})$, while the second is the covariance matrix arising from the Pauli basis, $(\frac{S_{hh}+S_{vv}}{\sqrt{2}}, \sqrt{2}S_{hv}, \frac{S_{hh}-S_{vv}}{\sqrt{2}})$. Both carry all the information about the polarimetric properties of a homogeneous distributed scatterer. From these matrices the polarimetric decompositions of van Zyl (1993), Cloude and Pottier (1997) and Freeman and Durden (1998) were calculated, and the decomposed data were converted to terrain-corrected data. To obtain 25 m ground-resolution, terrain-corrected polarimetric features, we used 6 looks with ALOS-1 (1 in range and 6 in azimuth) and 36 looks with ALOS-2 (4 in range and 9 in azimuth). The overall processing chain is illustrated in Fig. 2 and was implemented using SNAP (ESA's Sentinel Application Platform v9.0.0). More detailed information about the steps in Fig. 2 is available in standard SAR textbooks (Lee and Pottier, 2009; Richards, 2009).

2.3. Decompositions of full-polarimetric L-band SAR observations

The covariance and coherency matrices are used to gain information on the physical interactions occurring when distributed scatterers, such as vegetated regions, are imaged by the SAR system (Lee and Pottier, 2009). However, interpretation of these matrices is not straightforward due to the complexity of the scattering process and the variability of the scatterers within each pixel. Polarimetric decomposition techniques, building on a concept first introduced by Cloude (1985), have emerged as a basic tool aiding such interpretation. We use three decomposition methods, those of van Zyl (1993), Cloude and Pottier (1997) and Freeman and Durden (1998). This is because they make different assumptions and/or provide useful complementary information.

van Zyl (1993) used an eigen-decomposition of the covariance matrix to help interpret the scattering from natural terrain, especially vegetated areas. This decomposition considers scatterers with reflection symmetry (i.e., their statistical properties would be unchanged if they were reflected relative to the observation geometry; this is typical of most natural scenes, though topography can cause this condition to be violated). The eigenvectors of the covariance matrix are identified with three types of scattering mechanism: cross-polarized scattering and scattering involving either an odd or an even number of reflections,

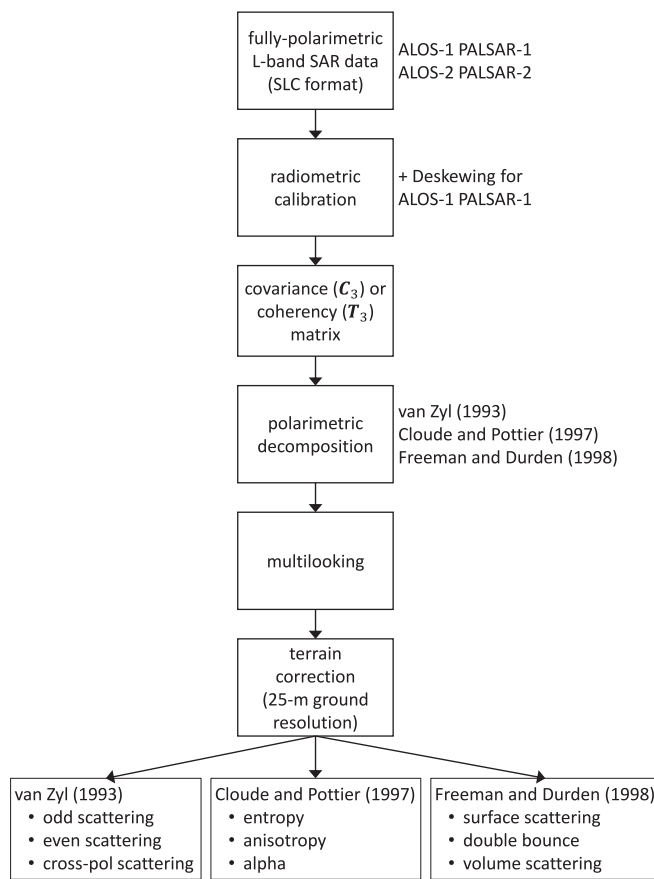


Fig. 2. Simplified processing chain for ALOS-1 PALSAR-1 and ALOS-2 PALSAR-2 fully-polarimetric data from single-look complex (SLC) format to terrain-corrected scattering mechanisms and parameters.

whose relative power is given by the eigenvalues. Later studies interpreted the cross-polarized return as volume scattering, with an odd number of reflections coming from surface scatter and an even number from double bounce scattering, not least because scattering models showed that these would be the dominant contributions to the observed backscatter. However, this does not follow from the van Zyl (1993) analysis, since it neglects the fact that scattering involving an even and odd number of reflections can also arise from the random volume making up the canopy and should be included in volume scattering.

Freeman and Durden (1998) addressed this issue with a model-based approach which explicitly calculates the covariance matrices arising from: (i) a collection of randomly oriented cylinders (corresponding to the volume scattering from the vegetation canopy); (ii) a set of vertical cylinders standing on flat ground (representing double bounce scattering); (iii) direct scatter from the ground, considered as a rough surface. The observed covariance matrix is assumed to be the sum of the individual covariance matrices corresponding to these three mechanisms. A crucial point is that this method calculates the *relative* powers in the three mechanisms, allowing the measured total power to be partitioned accordingly. However, while the volume scattering is unambiguously recovered, separating the double bounce from surface scatter requires the use of the phase of the HH-VV element of the covariance matrix. This can be understood roughly as the average phase difference between the HH and VV signals and borrows from the discussion in van Zyl (1993).

Cloude and Pottier (1997) developed a different physical basis on which to interpret the data by using the coherency matrix to calculate the entropy and alpha angle associated with an extended scatterer and associating these quantities with combinations of scattering mechanisms. The entropy-alpha plane identifies where the data lie relative to

specific zones characteristic of classes with different scattering behaviour.

The characteristics of each approach are briefly described in the Supplementary Information (Appendix 1), while detailed information can be found in the original publications (Cloude and Pottier, 1997; Freeman and Durden, 1998; van Zyl, 1993) or in reference books (Lee and Pottier, 2009; van Zyl and Kim, 2011).

2.4. Soil characteristics

L-band SAR data can be affected by edaphoclimatic factors (Lucas et al., 2010; Mattia et al., 1997). Estimates of soil moisture were obtained from the European Centre for Medium-Range Weather Forecasts (ECMWF) ERA5-Land product, a reanalysis dataset providing a consistent view of the evolution of land variables since 1950 at ~ 10 km spatial resolution (Muñoz-Sabater et al., 2021). This dataset was downloaded from Earth Engine Data Catalog (<https://developers.google.com/earth-engine/datasets/catalog/ECMWF ERA5 LAND HOURLY>). The volume of water in the 0–7 cm soil layer at the date of the observations was used as a proxy for soil moisture. Soil texture was obtained from ISRIC – World Soil Information's SoilGrids, a global gridded soil dataset at 250 m grid spacing (Poggio et al., 2021); sand content in the 0–5 cm soil layer was downloaded from Google Earth Engine as a community contributed dataset.

2.5. Modelling the determinants of L-band SAR backscatter in the dry tropics

To understand how vegetation and soil properties interact to determine the radar signal, we used structural equation models (SEM). SEM is an inference method aiming at testing a concept by specifying a conceptual model (i.e., Eq. (1) below) representing its predictions derived from suitable observational data (Pearl, 2012). To address the theoretical expectation that the radar signal is not directly related to AGBD (Brolly and Woodhouse, 2012), we model separately the effect of stem density and mean stem biomass (whose product is AGBD). The set of relationships between these factors and scattering mechanisms can be formalized by the following set of equations:

$$\{sur, vol, dbl\} = f_i(N, \bar{b}, soil_wat, soil_sand) \quad (1)$$

where *sur*, *vol*, and *dbl* refers to the three scattering mechanisms from (Freeman and Durden, 1998): surface scattering, volume scattering, and double bounce, respectively, *N* is stem density (stems ha^{-1}), \bar{b} is the mean stem biomass (t stem^{-1}), *soil_wat* is the soil volumetric water content ($\text{m}^3 \text{m}^{-3}$), *soil_sand* is the soil sand content (g kg^{-1}), and f_i is a linear function relating dependent variables and covariates. Vegetation water content is not explicitly included in the structural equation model because comparable in situ or remotely sensed vegetation water content products are not available at the spatial and temporal scales of our multi-continental dataset. Instead, we use soil volumetric water content as a proxy for dielectric variability, since variations in soil moisture generally exert the strongest control on L-band backscatter under dry-tropical and savanna conditions (Jackson and Schmugge, 1991; Ulaby et al., 1986). While vegetation water content can modulate canopy dielectric properties and thus volume scattering, its effect is secondary when soil water content is low. Furthermore, although precipitation can transiently wet foliage, in dry-tropical trees the vegetation water content remains relatively stable because the trees have to remain turgid even in dry spells/seasons (Vinya et al., 2019).

Fig. 3 shows the SEM representation of Eq. (1). Stem density and mean stem biomass were \log_2 transformed to improve the linearity of the relationships and to allow easy comparison of their effects (i.e., the size of the resultant effect on scattering mechanisms estimated by the model is the effect of doubling these variables). The other variables were standardized to z-scores to allow comparison of data across variables or

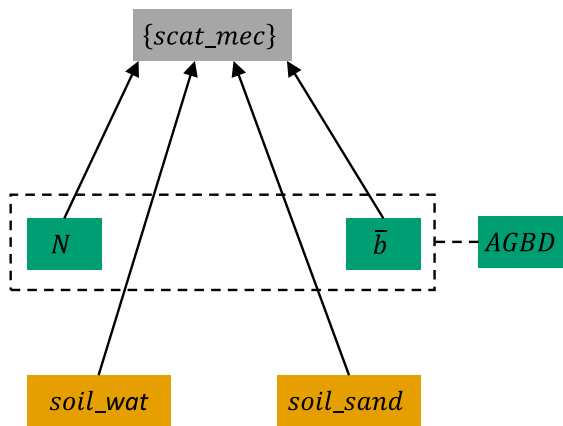


Fig. 3. Structural equation modelling (SEM) representation of Eq. (1): $scat_mec$ indicate scattering mechanisms; $AGBD$ - aboveground biomass density, N - stem density; \bar{b} - mean stem biomass; $soil_wat$ - volumetric soil water content; $soil_sand$ - soil sand content. N and \bar{b} are encompassed by a dashed rectangle to indicate that their product yields aboveground biomass density ($AGBD$).

datasets with different observational scales. The number of observations at each site ranged from 8 in Zimbabwe (ZFC) to 150 in Congo (CBN). We defined a weighted variable to address this unbalanced design such that each location had equal weight. A robust weighted least squares (WLS) estimator was used to accommodate weighted observations and account for violations of model assumptions, such as non-normality, non-linearity and non-constant variances (Kline, 2016). Model fitting was performed with the R (R Core Team, 2023) *lavaan* package (v 0.6–15) (Rosseel, 2012).

To visualise the relationships between the scattering mechanisms and the ground observations of vegetation structure we use generalized additive models (GAMs; Hastie and Tibshirani (1986)). We fit: $\{scat_mec\} = \beta_0 + s_1(vegStr) + s_2(vegStr, location) + \varepsilon$, with $vegStr$ referring to vegetation structure ($AGBD$, stem density or mean stem biomass). An adaptive smooth (s_1) was selected as the smoothing basis to allow the smoothness of the function to vary across the range of $vegStr$ values, thereby accommodating varying degrees of complexity in different regions of the data; s_2 is the factor-smooth interaction between $vegStr$ and location; ε is the error term. A 95 % confidence interval of the first derivative of the smooth function $s_1(vegStr)$ for each scattering mechanism is used to help detect saturation. When the first derivative of

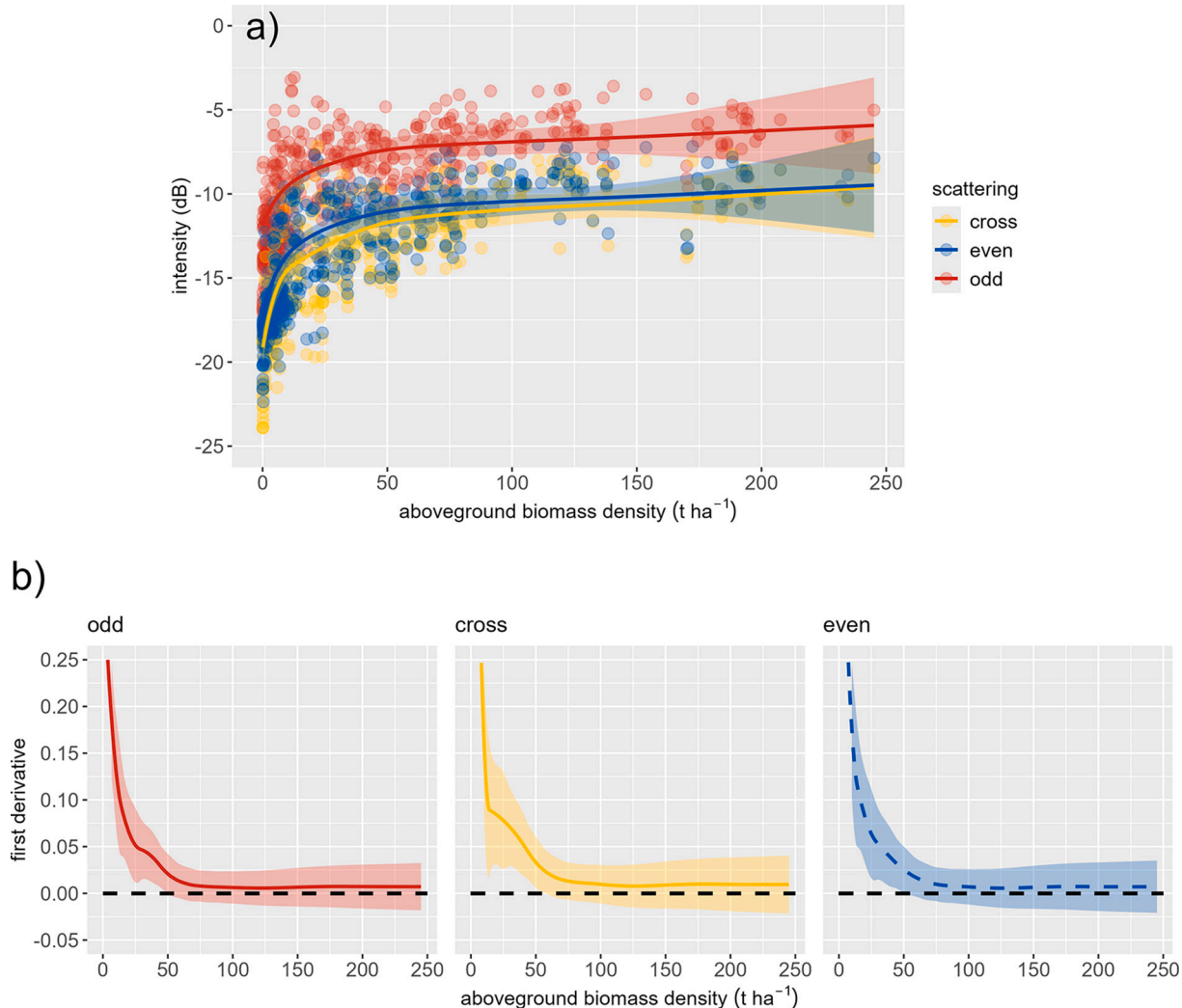


Fig. 4. a) Relationship between scattering mechanisms derived from the van Zyl polarimetric decomposition (van Zyl, 1993) applied to PALSAR-1 and PALSAR-2 fully-polarimetric observations and aboveground biomass density ($AGBD$); scattering mechanisms are represented as backscatter intensity (dB scale): *odd* - odd number of bounces, *even* - even number of bounces, *cross* – scattering in the cross-pol channel; the solid lines represent generalized additive model fits. b) Relationship between the first derivative of the smooth function $s_1(AGBD)$ and $AGBD$. Shaded areas represent 95 % confidence intervals.

a GAM fit includes zero, it indicates that from that *vegStr* value onwards, the response variable (scattering mechanism) is insensitive to *vegStr* (*AGBD*, stem density or mean stem biomass).

3. Results

3.1. Relationship between scattering mechanisms and vegetation structure

Fig. 4a shows the distribution of the intensity of the scattering mechanisms from van Zyl (1993) as a function of *AGBD*. The dominant mechanism is scattering by an odd number of bounces, which is likely to represent direct scattering from the ground together with scattering from branches in the canopy. There is a significant positive trend with *AGBD* up to 52 t ha^{-1} , 58 t ha^{-1} and 52 t ha^{-1} for odd, cross, and even scattering, respectively (Fig. 4b), after which there is no sensitivity. Cross-pol scattering and scattering by an even number of bounces are very similar to each other and their relation to *AGBD* closely follows that of scattering by an odd number of bounces, though with magnitude ~ 5 dB lower.

The Cloude and Pottier (1997) polarimetric decomposition (Fig. 5) shows that scattering is dominated by medium entropy vegetation scattering, with some medium entropy surface scattering at low and intermediate *AGBD* values. As expected, vegetation scattering tends to dominate as *AGBD* increases. Only two observations exhibit low entropy surface scattering (entropy < 0.5 and $\alpha < 42.5^\circ$), which is characteristic of very smooth ground surfaces (plots ABG_17 and ABG_19, *AGBD* = 0.1 and 0.3 t ha^{-1} , respectively), and only a single observation exhibits medium entropy multiple scattering (entropy = 0.5–0.9 and $\alpha > 50^\circ$), characteristic of double bounce scattering (plot TKW_8, *AGBD* = 23.1 t ha^{-1}).

Fig. 6a displays the relationships between the intensity of the scattering mechanisms obtained from the Freeman and Durden (1998) polarimetric decomposition and *AGBD*. Volume scattering is always the dominant mechanism, followed by double bounce, with surface scattering apparently not showing any relation with *AGBD*. The significance of the relationship between volume scattering and *AGBD* is only maintained up to 58 t ha^{-1} (Fig. 6b). There is no significant relationship between the intensity from surface scattering and *AGBD* (Fig. 6b), whereas for double bounce a positive trend is maintained for *AGBD* up to

22 t ha^{-1} . The results from the Freeman-Durden decomposition agree with those from the entropy/anisotropy/ α polarimetric decomposition (Fig. 5) in that the observed backscatter comes primarily from a mixture of volume and surface scattering, with volume scattering clearly being the dominant mechanism.

AGBD is the product of stem density and mean stem biomass, but these two variables are likely to influence the SAR signal in different ways (Brolly and Woodhouse, 2012; Smith-Jonforsen et al., 2007). Fig. 7a and b show the relationship between them and the intensity of each scattering mechanism from the Freeman-Durden polarimetric decomposition. Volume scattering increases with stem density up to $652 \text{ stems ha}^{-1}$ (Fig. 7c), after which sensitivity to stem density is lost. The intensity from double bounce increases with stem density up to $\sim 260 \text{ stems ha}^{-1}$, with surface scattering showing no sensitivity to stem density. Sensitivity of scattering mechanisms to mean stem biomass is much harder to interpret because most observations are aggregated around a similar mean stem biomass value (Fig. 7b). There is a large cluster of plots with mean stem biomass around 0.1 t stem^{-1} , i.e., corresponding to stems with $\sim 10 \text{ cm DBH}$. The only significant and positive trend is between the intensity from volume scattering and mean stem biomass. In contrast to the 10 dB range in the trend between the intensity from volume scattering and stem density, it has only a 5 dB range and considerably more dispersion. There is moderate evidence that surface scattering declines at high stem density, and a non-significant decline in double bounce above $300 \text{ stems ha}^{-1}$.

Fig. S3a-b (Supplementary Information) show scatterplots of the relationship between the intensity of scattering mechanisms from Freeman and Durden (1998) and soil characteristics: soil water content and soil sand content. The only clear behaviour regarding soil properties is that volume scattering increases as soil moisture increases; somewhat surprisingly, surface scattering does not increase as soil moisture increases.

3.2. Structural equation modelling

The path diagram from the structural equation model (SEM) resulting from Eq. (1) is shown in Fig. 8 for the Freeman and Durden (1998) polarimetric decomposition. The model has a *p*-value < 0.001 , suggesting that our dataset supports the fitted SEM. Volume scattering is the

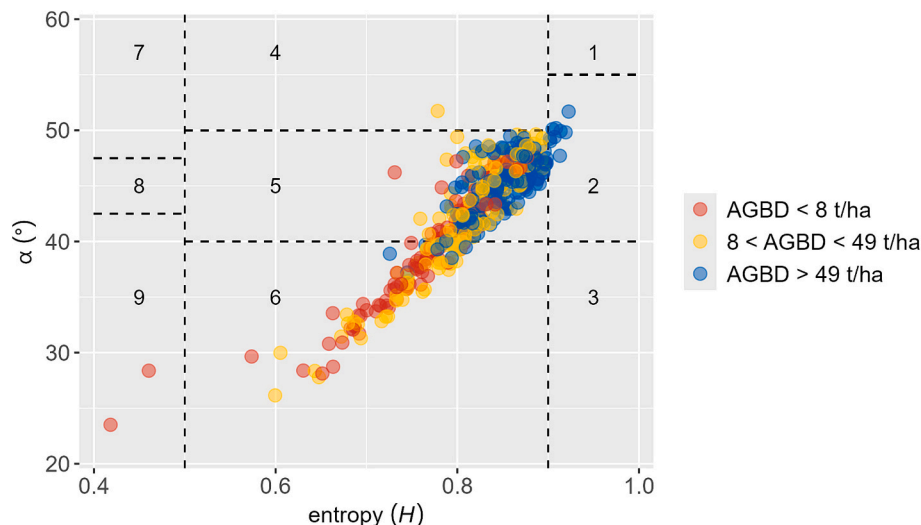


Fig. 5. Distribution of reference plots on the entropy (*H*) - α ($^\circ$) plane obtained from the Cloude and Pottier (1997) polarimetric decomposition (see Fig. 5). The colour of each point is a function of aboveground biomass density (*AGBD*) terciles: red: $AGBD < 8 \text{ t ha}^{-1}$, yellow: $8 < AGBD < 49 \text{ t ha}^{-1}$, blue: $AGBD > 49 \text{ t ha}^{-1}$. The black dashed lines represent the nine different scattering zones according to Cloude and Pottier (1997): 1 - high entropy multiple scattering, 2 - high entropy vegetation scattering, 3 - (non-feasible) high entropy surface scattering, 4 - medium entropy multiple scattering, 5 - medium entropy vegetation scattering, 6 - medium entropy surface scattering, 7 - low entropy multiple scattering events, 8 - low entropy dipole scattering, 9 - low entropy surface scattering. (For interpretation of the references to colour in this figure legend, the reader is referred to the web version of this article.)

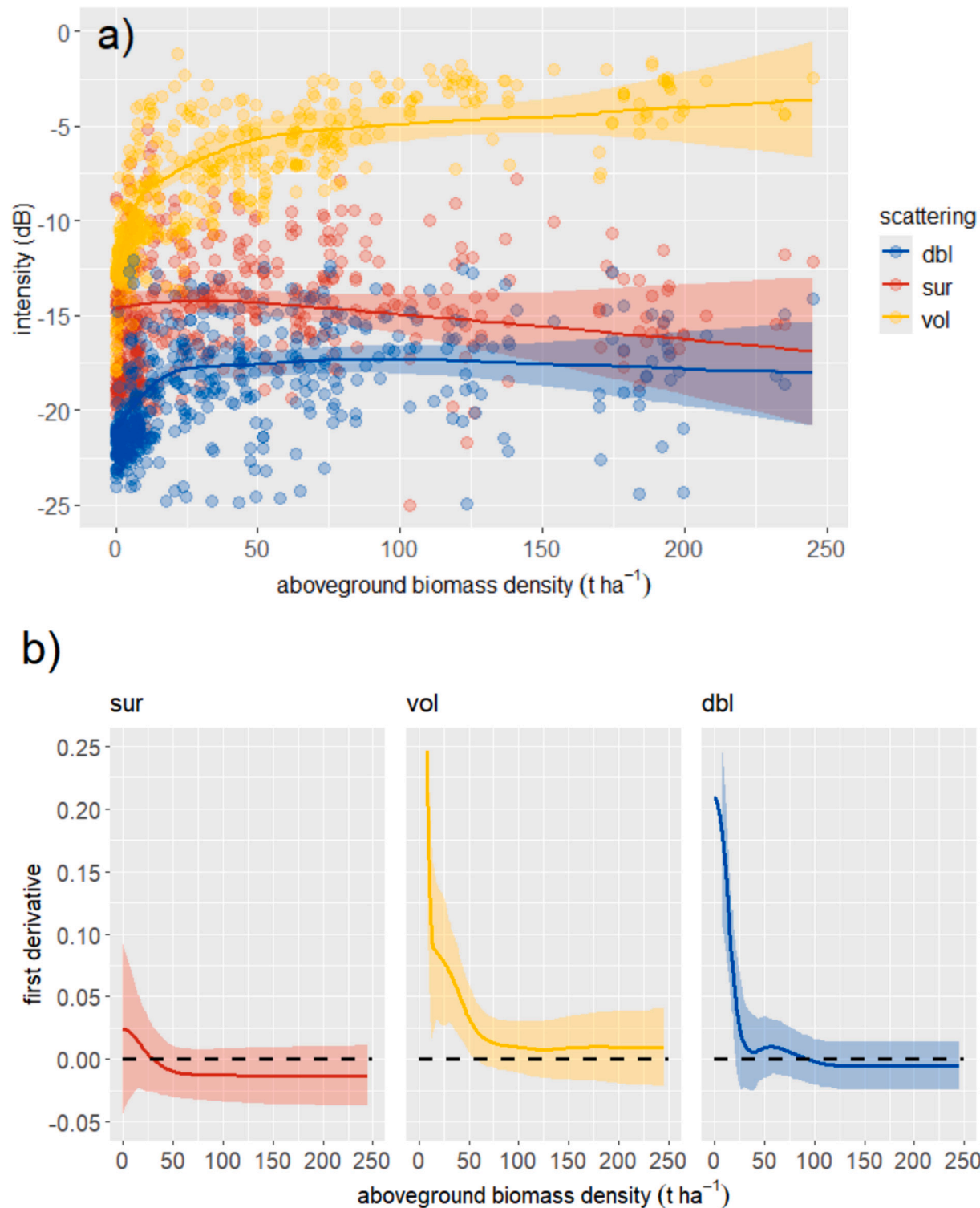


Fig. 6. a) Relationship between scattering mechanisms derived from the Freeman-Durden polarimetric decomposition (Freeman and Durden, 1998) applied to PALSAR-1 and PALSAR-2 fully-polarimetric observations and aboveground biomass density (AGBD); scattering mechanisms are represented as backscatter intensity (dB scale): sur – surface scattering, vol – volume scattering, dbl – double bounce scattering; the solid lines represent generalized additive model fits. b) Relationship between the first derivative of the smooth function $s_1(AGBD)$ and AGBD. Shaded areas represent 95 % confidence intervals.

mechanism most sensitive to vegetation structure, especially to stem density, as it increases by 0.32 standard deviations (SDs) for each doubling of stem density. The effect of mean stem biomass on volume scattering is much smaller (0.14 SD for each doubling of mean stem biomass). The strongest effect from soil variables on volume scattering comes from soil water content (0.23 SD increase in volume scattering for

each SD increase of soil moisture). Double bounce scattering is strongly affected by stem density (0.25 SD increase of double bounce for each doubling of stem density). Soil sand content has a moderate negative effect on double bounce (-0.18 SD). The only significant effect on surface scattering comes from stem density, a positive effect of 0.08 SD.

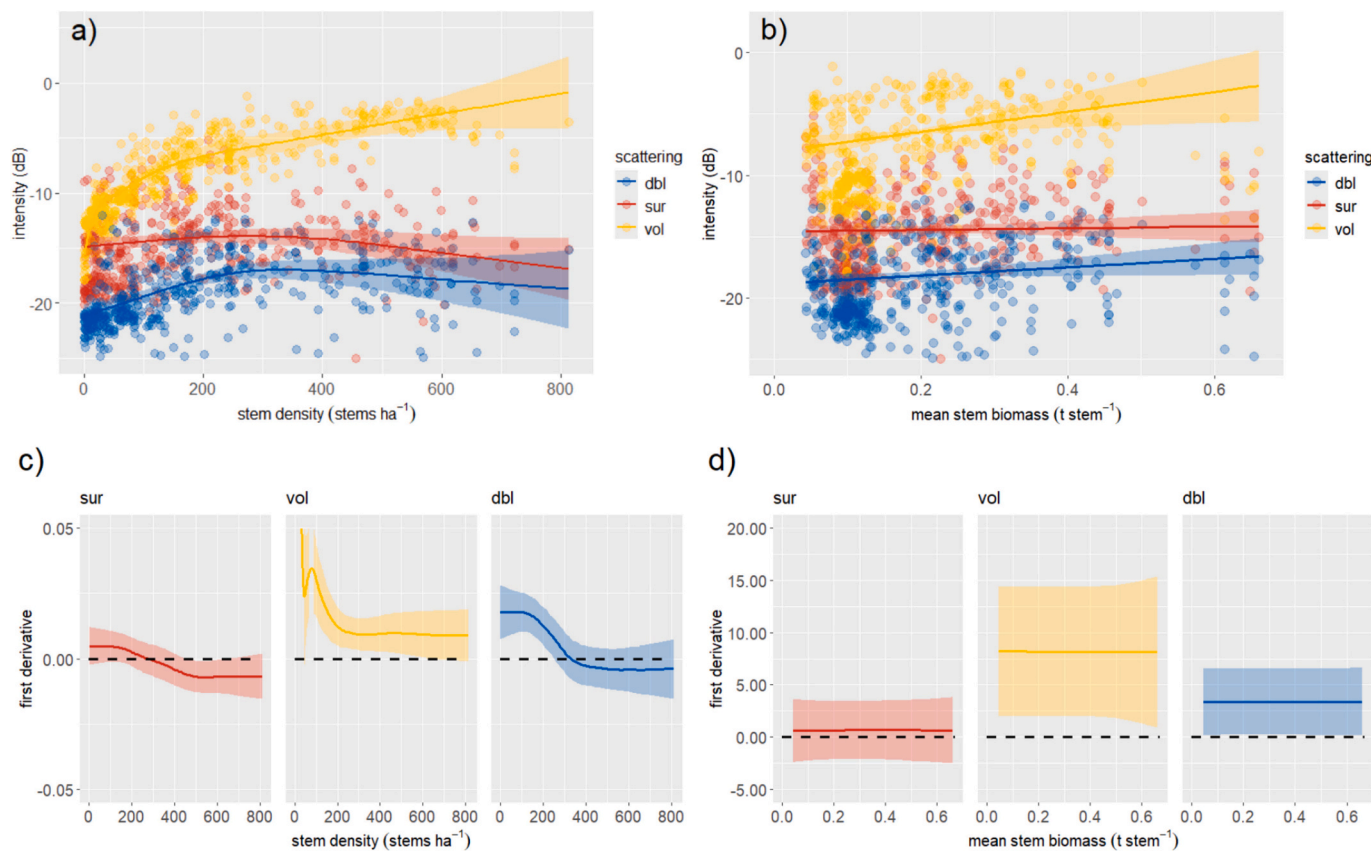


Fig. 7. Relationship between scattering mechanisms derived from the Freeman-Durden polarimetric decomposition (Freeman and Durden, 1998) applied to PALSAR-1 and PALSAR-2 fully-polarimetric observations and a) stem density (N), b) mean stem biomass (\bar{b}); scattering mechanisms are represented as backscatter intensity (dB scale): sur – surface scattering, vol – volume scattering, dbl – double bounce scattering; the solid lines represent generalized additive model fits. c) relationship between the first derivative of the smooth function $s_1(N)$ and N ; d) relationship between the first derivative of the smooth function $s_1(\bar{b})$ and \bar{b} . Shaded areas represent 95 % confidence intervals.

4. Discussion

4.1. Dominant scattering mechanisms in the dry tropics

Across our dataset, most plots were characterized by medium entropy vegetation scattering, although for sites with lower stem densities / AGBD the balance shifted towards medium entropy surface scattering. Such behaviour is likely to be typical of the dry tropics since our dataset includes most wooded types in this region. Medium entropy implies that more than one scattering mechanism is important, suggesting that investigation of vegetation properties will usually have to contend with a soil component in the L-band SAR signal.

Comparison with the findings in van Zyl (1989) and van Zyl (1993) suggests that the scattering at our study locations is intermediate between that of short shrub-like vegetation and dense forest (though the van Zyl studies dealt with coniferous forest). For the shrubby area discussed in van Zyl (1993) the power due to an odd number of reflections was 2.0 and 2.2 times higher than from an even number of reflections and cross-pol scattering, respectively, and 2.7 and 3.7 times higher for the forested area, while our study gives values of 2.4 and 2.8 after averaging across all observations. This is likely to be a consequence of stem properties: density, size and shape. In particular, van Zyl (1993) concluded that most of the scattering in the shrubby area came from vegetation with randomly oriented branches that were thin compared to the radar wavelength, while in the forested area it was dominated by scattering from the randomly oriented cylinders composing the branches.

The structural inferences from van Zyl (1993) are more specifically

embedded in the Freeman and Durden (1998) decomposition, which assumes that:

- volume (vegetation canopy), surface and double bounce scattering are the three main scattering mechanisms, and these add incoherently (more complete radiative transfer models would show the same);
- branches are randomly oriented and thin compared to the SAR wavelength;
- double bounce comes from a vertically oriented trunk on a flat ground, so would be much weaker in vegetation with a multi-stem structure or on sloping ground.

Particularly important is that the second assumption is likely to be true in the wooded vegetation we are studying, given the 24 cm L-band wavelength and the moderate AGBD levels (median = 23.1 t ha⁻¹, standard deviation = 53.8 t ha⁻¹). It is similar to van Zyl's inference about scattering from a shrubby area (van Zyl, 1993), and specifically allows the contributions to volume scattering of the HH, HV and VV returns to be calculated.

At our sites, volume scattering is clearly identified as the dominant mechanism over the wooded vegetation types, though it is mixed with a weaker return from surface scattering and, in most cases, a much weaker return from double bounce (Fig. 6). Somewhat surprising is that volume scattering is present even at very low levels of AGBD. This is unlikely to be a soil roughness effect since most soil surfaces in this region would be perceived as smooth by the 24 cm wavelength of the L-band sensor. However, it could be an effect of surface slopes, in particular aspect

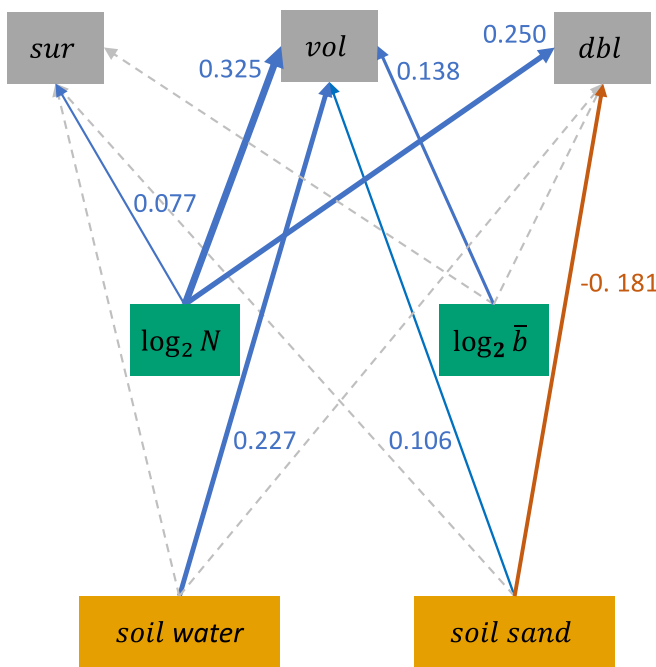


Fig. 8. Path diagram of the fitted structural equation model with \log_2 stem density (N) and \log_2 mean stem biomass (\bar{b}) as vegetation covariates. The numerical values indicate size effects, i.e. by how many standard deviations (SDs) the backscatter intensity changes by due to a change of 1 SD in the soil variables or a doubling of the vegetation variables (N and \bar{b}) (blue: positive effect; orange: negative effect; the line width is proportional to the size of the effect). Non-significant estimates are indicated by grey dashed lines. Freeman and Durden (1998) scattering mechanisms: *sur* - surface scattering, *vol* - volume scattering, *dbl*: double bounce. Soil variables: *soil water* - volumetric soil water content, *soil sand* - soil sand content. (For interpretation of the references to colour in this figure legend, the reader is referred to the web version of this article.)

angle. It could also be the signal from the small trees and shrubs that are not included in our *AGBD* estimate, i.e. are less than 10 cm DBH. More detailed knowledge of the vegetation and soil structure at these low *AGBD* sites would be needed to establish whether this is really a signal from the vegetation canopy. The low importance of double bounce is probably because of weaker scatter from dry soils, the presence of tree types that often lack a single vertical stem (Conti et al., 2019), and in some cases the effect of surface slopes (the double bounce mechanism weakens sharply as the angle between the stem and ground surface deviates from 90°).

Volume scattering tends to dominate in the figures above because the plots are wooded, but Fig. 9 from the Mozambique site (Gorongosa National Park, MGR) illustrates that this is not just a feature of the plots but is a distinctive characteristic of the landscape and is not simply an artefact of the Freeman-Durden decomposition. Wooded pixels, shown as green in the Landsat 5 Thematic Mapper (TM) image (Fig. 9b) correspond to pixels dominated by volume scattering in ALOS (Fig. 9a) while bare soil pixels (bright red/pink in TM) relate to pixels dominated by surface scattering for ALOS. Regions characterized by mixed tree species and low canopy cover (reddish in TM) tend to exhibit a mixture of volume and surface scattering (yellow in ALOS). Double bounce is the dominant mechanism in only 0.07 % of the pixels in this scene.

The relationship between *AGBD* and the Freeman and Durden (1998) decomposition is consistent with what would be expected on physical grounds. According to the fitted GAM, volume scattering is sensitive to *AGBD* up to ~ 60 t ha^{-1} (Fig. 6a and b), whereas double bounce has a significantly lower *AGBD* saturation level (22 t ha^{-1}). Surface scattering has no significant relationship with *AGBD* (Fig. 6b). This can be interpreted as: a) the intensity from volume scattering and double bounce mechanisms increases with *AGBD* up to ~ 25 t ha^{-1} , as lower stem density values allows the signal to penetrate down to the soil surface and return to the sensor through double bounce; b) as *AGBD* increases, the signal is more and more attenuated as it traverses the canopy, causing surface scattering and double bounce to be reduced. Furthermore, there is also a significant positive correlation between *AGBD* and soil moisture ($R = 0.399$, Supplementary Information Fig. S4), an indication of wetter soil conditions supporting higher *AGBD*. There is no evidence of a strong impact of soil moisture on scattering mechanisms (Supplementary Information Fig. S3a), supporting the work of, e.g., Gou et al. (2022). Also, vegetation moisture changes tend to be small in dryland forests and have little effect on L-band backscatter, unlike effects observed in other biomes (Monteith and Ulander, 2018).

Further insight into the relationship between *AGBD* and the fully-polarimetric SAR return is provided by considering the individual channels (Fig. 10; compare with Fig. 6). Volume scattering and HV backscatter display similar relationships with *AGBD*, differing only in terms of their magnitude. This is a consequence of the Freeman and Durden (1998) decomposition including contributions from the cross- and co-polarized channels in volume scattering. Eq. (17) (Supplementary Information Appendix 1) indicates that the total volume scattering should be 4 times (about 6 dB) greater than the cross-pol scattering, which is roughly consistent with what is observed.

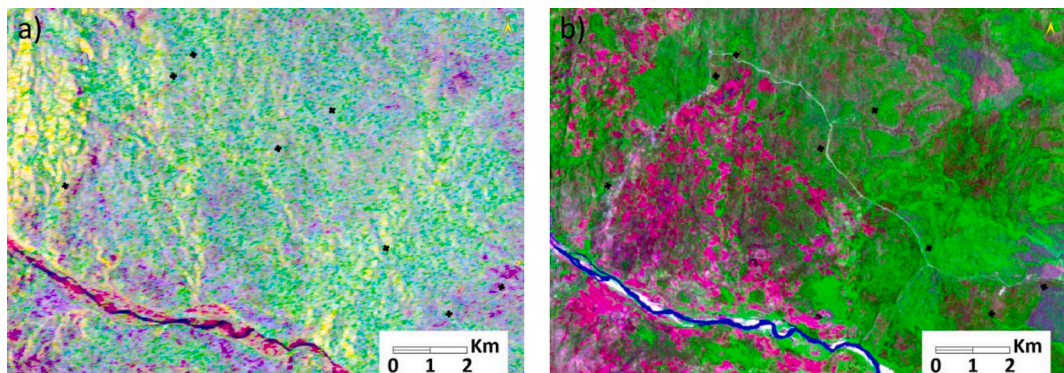


Fig. 9. Colour composite image (RGB) displaying a) scattering mechanisms obtained from the Freeman and Durden (1998) decomposition; red: surface scattering, green: volume scattering, blue: double bounce. b) surface reflectance obtained from Landsat 5 Thematic Mapper (TM); red: shortwave infrared band, green: near infrared band, blue: green band. a) and b) were acquired over the Mozambique location (Gorongosa National Park, MGR): ALOS PALSAR scene ALPSRP201996810 from 8 November 2009 and Landsat 5 TM scene LT05_L2SP_167073_20091129_20200825_02_T1 from 29 November 2009, respectively. The eight black spots depict the 1-ha plots in this scene. (For interpretation of the references to colour in this figure legend, the reader is referred to the web version of this article.)

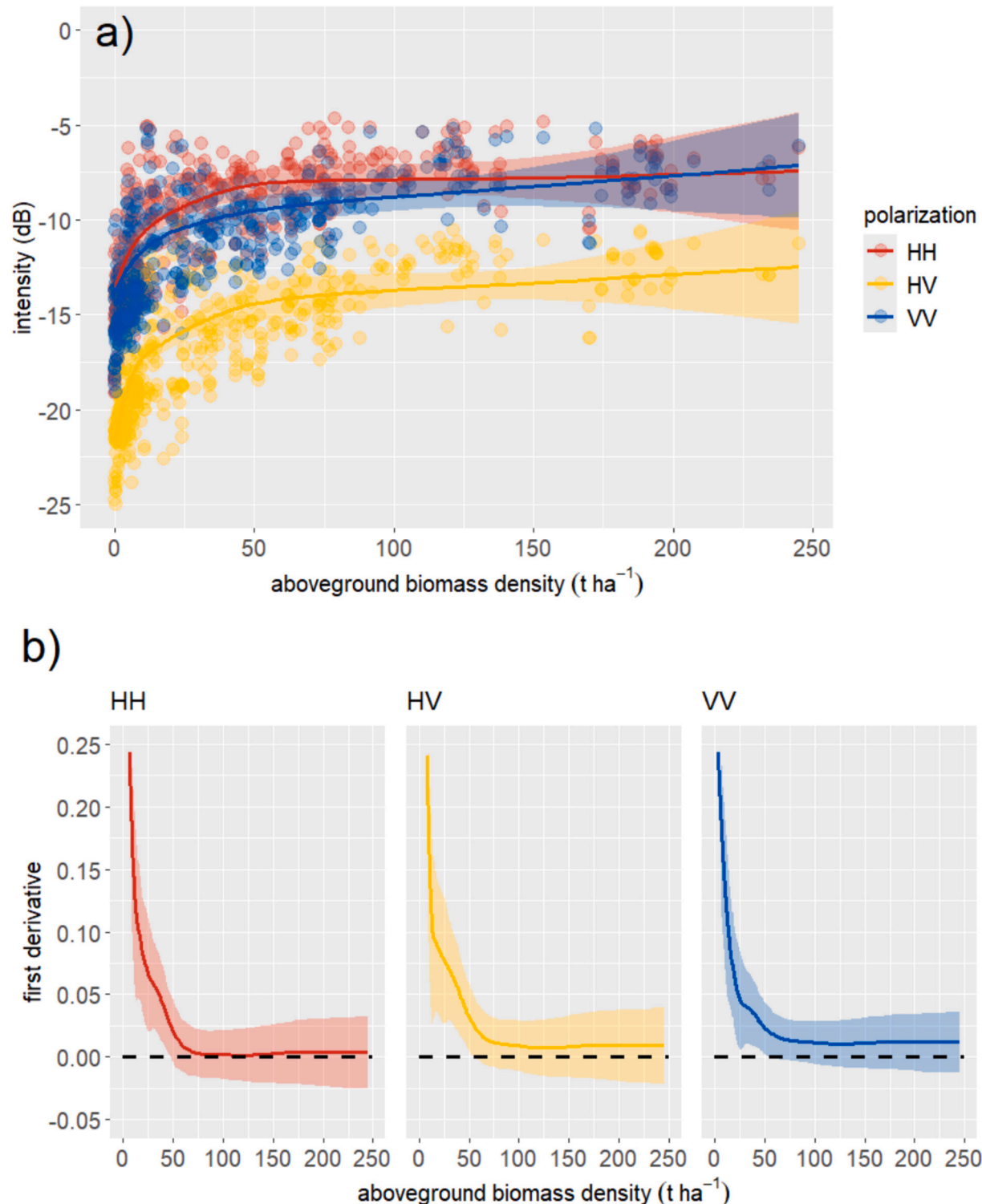


Fig. 10. a) Relationship between individual polarizations from PALSAR-1 and PALSAR-2 fully-polarimetric observations and aboveground biomass density (AGBD); polarizations are represented as backscatter intensity (dB scale); the solid lines represent generalized additive model fits, using an adaptive smooth as smoothing basis. b) Relationship between the first derivative of the smooth function s_1 (AGBD) and AGBD. Shaded areas represent 95 % confidence intervals.

4.2. Determinants of scattering mechanisms: vegetation structure vs environmental conditions

The SEM path diagram (Fig. 8) shows the significant effects indicated by the data within the model structure imposed by Eq. (1). The values on the diagram should be interpreted as conditional sensitivities, i.e., where an arrow connects box x to box y , the size effect is an estimate of dy/dx (with the units of x and y either scaled or \log_2 transformed) when other variables are held at their mean. Stem density is seen to be the main vegetation driver of volume and double bounce scattering; this is not unexpected as both rely on scattering involving the canopy. Mean stem biomass affects volume scattering but not double bounce or surface scattering, and its effect is weaker than stem density. The relative insensitivity of volume scattering to mean stem biomass may reflect that

dx (with the units of x and y either scaled or \log_2 transformed) when other variables are held at their mean. Stem density is seen to be the main vegetation driver of volume and double bounce scattering; this is not unexpected as both rely on scattering involving the canopy. Mean stem biomass affects volume scattering but not double bounce or surface scattering, and its effect is weaker than stem density. The relative insensitivity of volume scattering to mean stem biomass may reflect that

volume scattering would be expected to arise from randomly oriented branches, so is not directly related to stem properties.

Other things being equal, surface scattering should increase as soil water content increases, but there is no evidence for this (Supplementary Information Fig. S3a); instead, the only significant effect of increasing soil water content is to increase volume scattering. Two factors may help explain this: (i) the instantaneous value of soil water content, as used in Eq. (1) and Fig. 8, may indicate locations where the soils are generally wetter, so are able to support more vigorous growth and higher *AGBD*; this is supported by the fact that *AGBD* and *N* are both correlated with soil water content (0.40 and 0.47, respectively, Supplementary Information Fig. S4); (ii) in the data used, soil wetness is modelled on the basis of rainfall, but rain may also enhance volume scattering through water in the canopy. Again, Supplementary Information Fig. S4 shows that if soil moisture is small, *AGBD* and *N* are smaller; it is only as soil moisture gets to higher values that higher *N* and *AGBD* are seen. This suggests that the rain signature is an indicator of more general favourable growing conditions. Both effects would reduce surface scattering because of increased attenuation of the signal traversing the canopy.

Two L-band ALOS sensors with full-polarimetric capabilities were used in this study to obtain polarimetric features from several decompositions (Cloude and Pottier, 1997; Freeman and Durden, 1998; van Zyl, 1993). PALSAR-2 offers substantially finer resolution capability than PALSAR-1, largely because of wider supported bandwidths (14 MHz for PALSAR-1 and 28 MHz for PALSAR-2 when operating in full-polarimetric mode). This has implications when processing SAR data from slant-range SLC to terrain-corrected polarimetric features. To obtain terrain-corrected polarimetric features at 25-m ground resolution, 6 looks were applied to PALSAR-1 data (1 in range \times 6 in azimuth) and 36 looks to PALSAR-2 data (4 in range \times 9 in azimuth). The resulting values were then averaged at the plot level (1 ha, except for the 0.5 ha plots within caatinga vegetation in north-eastern Brazil), corresponding to approximately sixteen pixels per plot. Consequently, the equivalent number of looks (ENL) differs between sensors, which influences the degree of speckle-induced variability and may partly explain the observed dispersion in the data.

We cannot rule out limitations linked to the quality and spatial resolution of the covariates included in the SEM model (Fig. 8). *AGBD* was estimated from in situ measurements, with approximately 86 % of observations collected in 1 ha plots. Rejou-Mechain et al. (2014) reported that *AGBD* estimates from 1 ha plots have an average coefficient of variation of 17 %, compared with 46 % for 0.1 ha plots, as larger plots help minimise local spatial variability in stem biomass. Soil moisture was retrieved from the ECMWF ERA-5 Land product (Muñoz-Sabater et al., 2021), generated at \sim 10 km grid spacing, which for some sites may result in identical soil water content estimates across multiple plots. Soil texture data were obtained from ISRIC SoilGrids (Poggio et al., 2021), providing global coverage at 250 m resolution using a combination of field observations and EO-derived covariates; however, these may not fully capture local variation at specific sites.

The analysis of the relative importance of vegetation structure and soil characteristics in controlling L-band backscatter is therefore constrained by the limited spatial and temporal resolution of available soil data. In particular, soil surface roughness and near-surface soil moisture, both known to influence L-band backscatter, are difficult to measure at the time of satellite overpasses, and most datasets lack sufficient coverage to represent these variables reliably. Consequently, the weaker apparent contribution of soil properties in our results may reflect limitations in data availability rather than a lack of physical relevance. Future studies would benefit from targeted field campaigns coinciding with satellite acquisitions to enable a more robust assessment of soil influences on backscatter signals.

4.3. Implications for mapping aboveground biomass density

We find that, in the dry tropics, backscatter intensity from volume scattering, and more broadly from the cross-pol (HV) channel, is about twice as sensitive to stem density as to mean stem biomass. This suggests that *AGBD* maps based on radar intensity alone show too little change if *AGBD* is changing due to stems getting bigger, and it might overestimate changes with increases (decreases) in *AGBD* if driven by recruitment of new stems (or the loss of existing stems, through e.g. selective logging).

The findings from this study can help us propose several alternative approaches to *AGBD* mapping.

- (i) Availability of full-polarimetric observations and therefore, decomposition of the radar signal into volume scattering, surface scattering and double bounce offers the potential to invert the structural equation model and retrieve both stem density and mean stem biomass. This confers an advantage compared to retrieving only *AGBD* as a more complete description of forest structure can be generated, although the sensitivity to stem density becomes much weaker as stem density becomes large (Fig. 7). This approach requires full-polarimetric data which ALOS-4 PALSAR-3, ROSE-L and SAOCOM have capabilities to provide. The recently launched ESA BIOMASS mission will also acquire systematic fully polarimetric data but with a P-band radar (Quegan et al., 2019). However, our structural equation modelling framework is inherently independent of frequency. While the relative magnitudes of surface, volume, and double-bounce scattering will differ at P-band (owing to longer wavelength penetration and altered vegetation and soil interactions), the same physical decomposition principles and model structure apply.
- (ii) Taller trees generally contribute greater biomass (e.g., Duncanson et al. (2010)), so lidar observations of vegetation height could potentially support independent retrieval of mean stem biomass. Combining this with retrieval of stem density by inverting the structural equation model then provides a route to overall *AGBD*. However, the viability of this approach depends on the strength of the relationship between stem biomass and height, which is likely to vary across a landscape due to variations in tree structure and wood density. In addition, at present it could only be undertaken at local to regional scale using airborne scanning lidar, since spaceborne lidar, such as GEDI, only provides spaced samples of vegetation height.

4.4. The role of dual-pol L-band radar

Coverage of the dry tropics by fully polarimetric data is limited and will remain so. Therefore, global coverage of this biome may require exploitation of dual-polarized HH and HV data provided by JAXA, either mosaics from fine-beam scenes or ScanSAR observations (Koyama et al., 2019; Shimada et al., 2014; Shimada and Ohtaki, 2010). In this case Eqs. (14)–(17) (Supplementary Information Appendix 1) need to be modified to describe the associated 2-D covariance matrix, C_2 :

$$C_2 = C_{2s} + C_{2d} + C_{2v} \quad (2)$$

$$C_{2s} = f_s \begin{bmatrix} |\beta|^2 & 0 \\ 0 & 0 \end{bmatrix} \quad (3)$$

$$C_{2d} = f_d \begin{bmatrix} |\kappa|^2 & 0 \\ 0 & 0 \end{bmatrix} \quad (4)$$

$$C_{2v} = f_v \begin{bmatrix} 3/8 & 0 \\ 0 & 1/8 \end{bmatrix} \quad (5)$$

As for full polarimetry, the total volume scattering is four times greater than the HV scattering. The remainder after subtracting $3f_v/8$

from the *HH* power is the sum of surface and double bounce scattering terms, but without the *VV* return these can no longer be physically separated. However, the analysis above indicates that this remainder is usually dominated by surface scattering, at least in the dry woodlands comprehensively represented in our plot data.

While dual-polarimetric (*HH* and *HV*) data are more widely available than full-polarimetric acquisitions, their use in backscatter decomposition remains constrained. Recent work by [Mascolo et al. \(2022\)](#) demonstrates progress in adapting model-based decomposition to dual-pol data, particularly through separating volume and polarized contributions to the backscattered signal. However, they also highlight key limitations, such as the inability of the *HV* channel to reliably represent volume scattering, and the potential for misinterpretation of radar vegetation indices if the polarized contribution is not properly accounted for. These findings reinforce the difficulty of extracting physically meaningful scattering components from dual-pol observations, particularly in forested landscapes. Consequently, full-polarimetric SAR data remain essential for robust decomposition and interpretation of scattering mechanisms relevant to biomass estimation.

Currently, full-polarimetric data is only available roughly annually from PALSAR-2 and PALSAR-3. In contrast, dual-pol L-band SAR data from, e.g., PALSAR-2 and PALSAR-3 ScanSAR and soon NISAR, is/will be available at monthly or higher temporal frequencies. This raises the question of the trade-off between high temporal frequency dual pol and the increased information content of full-polarimetric data. It is likely that multi-annual data mostly improves *AGBD* mapping through a mixture of a) reduced uncertainty in the backscatter estimate through the suppression of speckle and other noise, and b) by providing data when soils are dry and thus contribute less to the signal ([Lucas et al., 2010](#)). In contrast, full-polarimetric data, as we show here, contains information about the vegetation structure beyond just *AGBD*, which should help to remove the systematic biases created by inconstancy in the vegetation structure-*AGBD* relationship, which likely create systematic biases in time and space. Thus, retrieving *AGBD* with these two approaches likely trades off random error (lower with multi-temporal dual pol) with systematic errors (lower with annual full-polarimetric data). The optimum solution would be to combine the two approaches in the future to minimise both kinds of errors, and this is an area for further work.

5. Conclusions

This study improves the understanding of how L-band SAR backscatter is related to woody vegetation structure and soil properties in dry tropical ecosystems, a crucial knowledge gap for accurate *AGBD* estimation, and a vital part of the land component in the global carbon cycle.

Our analysis, utilizing high-quality ground observations from multiple continents and corresponding fully-polarimetric ALOS L-band SAR data, reveals several key findings. First, volume scattering is the dominant scattering mechanism in wooded areas, even at low levels of *AGBD*. Second, a theory-informed structural equation model identifies stem density as the strongest determinant of volume scattering, followed by soil moisture, sand content, and mean stem biomass. Finally, double bounce scattering is usually of lower importance but exhibits significant correlations with both stem density and soil sand content. It may therefore be possible to retrieve multiple aspects of vegetation structure from polarimetric SAR observations, which could allow SAR observations to provide a novel and unique contribution to understanding the global carbon cycle and forest management.

Given the current limitations of dual-pol decomposition techniques, full-polarimetric data remain critical for reliably capturing vegetation scattering behaviour. Our results reinforce the importance of investing in and prioritising quad-pol SAR missions to advance large-scale biomass monitoring.

Given our findings about the importance of surface scattering, future

work should ensure that ground reference sites in the dry tropics include estimates of soil roughness (at relevant wavelengths), soil moisture and soil texture, as this would remove the need to use global coarse resolution estimates of soil properties. Similarly, it will be important to at least subsample the smaller vegetation which might be involved in volume scattering at low *AGBD*.

While limitations, such as potential site-specific variations, warrant further investigation, the established relationships demonstrate the significant promise of L-band SAR for improved *AGBD* estimation in dry tropical regions, ultimately contributing to a more comprehensive understanding of the global carbon cycle.

CRediT authorship contribution statement

João M.B. Carreiras: Writing – review & editing, Writing – original draft, Methodology, Investigation, Formal analysis, Data curation, Conceptualization. **Thomas Higginbottom:** Writing – review & editing, Methodology, Investigation. **John L. Godlee:** Writing – review & editing, Methodology, Data curation. **Sam Harrison:** Writing – review & editing. **Lorena Benitez:** Writing – review & editing. **Penelope J. Mograbi:** Writing – review & editing, Data curation. **Aurora Levesley:** Writing – review & editing, Data curation. **Karina Melgaço:** Writing – review & editing, Data curation. **David Milodowski:** Writing – review & editing. **Georgia Pickavance:** Writing – review & editing, Data curation. **Geoff Wells:** Writing – review & editing, Methodology. **Edmar Almeida de Oliveira:** Writing – review & editing, Data curation. **Luzmila Arroyo:** Writing – review & editing, Data curation. **Sam Bowers:** Writing – review & editing, Data curation. **Roel J.W. Brienen:** Writing – review & editing, Data curation. **Domingos Cardoso:** Writing – review & editing, Data curation. **António Alberto Jorge Farias Castro:** Writing – review & editing, Data curation. **Ezequiel Chavez:** Writing – review & editing, Data curation. **Ítalo A.C. Coutinho:** Writing – review & editing, Data curation. **Tomás F. Domingues:** Writing – review & editing, Data curation. **Fernando Elias:** Writing – review & editing, Data curation. **Mário Marcos Espírito Santo:** Writing – review & editing, Data curation. **Ted R. Feldpausch:** Writing – review & editing, Data curation. **David Galbraith:** Writing – review & editing, Data curation. **Emanuel Gloor:** Writing – review & editing, Data curation. **Francisco M.P. Gonçalves:** Writing – review & editing, Data curation. **Tatenda Gotore:** Writing – review & editing, Data curation. **Francoise Yoko Ishida:** Writing – review & editing, Data curation. **Timothy J. Killeen:** Writing – review & editing, Data curation. **Yadvinder Malhi:** Writing – review & editing, Data curation. **Beatriz S. Marimon:** Writing – review & editing, Data curation. **Ben Hur Marimon-Júnior:** Writing – review & editing, Data curation. **Desirée Marques Ramos:** Writing – review & editing, Data curation. **Simone Matias de Almeida Reis:** Writing – review & editing, Data curation. **Ian McNicol:** Writing – review & editing, Data curation. **Edward T.A. Mitchard:** Writing – review & editing, Data curation. **Peter Moonlight:** Writing – review & editing, Data curation. **Paulo S. Morandi:** Writing – review & editing, Data curation. **Patricia Morellato:** Writing – review & editing, Data curation. **Anderson Muchawona:** Writing – review & editing, Data curation. **Jonathan Muledi:** Writing – review & editing, Data curation. **Alejandro Murakami:** Writing – review & editing, Data curation. **Mylor Ngoy Shutcha:** Writing – review & editing, Data curation. **Paula Nieto-Quintano:** Writing – review & editing, Data curation. **Alexander Parada-Gutierrez:** Writing – review & editing, Data curation. **Nayane Cristina Candida dos Santos Prestes:** Writing – review & editing, Data curation. **Luciano Paganucci de Queiroz:** Writing – review & editing, Data curation. **Priscila M.S. Rodrigues:** Writing – review & editing, Data curation. **Jhonathan Oliveira Silva:** Writing – review & editing, Data curation. **Rubens M. Santos:** Writing – review & editing, Data curation. **Tiina Särkinen:** Writing – review & editing, Data curation. **Domingos Fortunato P.F. Silva:** Writing – review & editing, Data curation. **Tony C. de Sousa Oliveira:** Writing – review & editing, Data curation. **Marc Steininger:** Writing – review & editing, Data curation.

José Tchamba: Writing – review & editing, Data curation. **Elmar Veenendaal:** Writing – review & editing, Data curation. **Débora Zuanny:** Writing – review & editing, Data curation. **Tim R. Baker:** Writing – review & editing, Funding acquisition. **Kyle G. Dexter:** Writing – review & editing, Funding acquisition, Data curation. **Gabrielle Hegerl:** Writing – review & editing, Funding acquisition. **R. Toby Pennington:** Writing – review & editing, Funding acquisition. **Oliver L. Phillips:** Writing – review & editing, Funding acquisition. **Stephen Sitch:** Writing – review & editing, Funding acquisition. **Mathew Williams:** Writing – review & editing, Funding acquisition, Data curation. **Shaun Quegan:** Writing – review & editing, Writing – original draft, Methodology, Funding acquisition, Conceptualization. **Casey M. Ryan:** Writing – review & editing, Writing – original draft, Methodology, Funding acquisition, Data curation, Conceptualization.

Declaration of competing interest

The authors declare that they have no known competing financial interests or personal relationships that could have appeared to influence the work reported in this paper.

Acknowledgments

UKRI NERC grants for SEOSAW (A Socio-Ecological Observatory for the Southern African Woodlands; NE/P008755/1), and SECO (Resolving the current and future carbon dynamics of the dry tropics, NE/T01279X/1) and NERC NE/W001691/1; NE/N011570/1). Data collection from CAA plots was supported by the São Paulo Research Foundation (FAPESP), grant number #2015/50488-5) and NERC (grant number NE/N012488/1). Jon Lloyd is particularly acknowledged for providing access to field data collected at several plots in Latin America: BTI-01, CJU-01, GBR-01, GBR-02, IBD-01, IBD-02, JUV-01, MOR-01, MOR-02, PSC-01, PSC-02, PSC-03, SDA-01, SDA-02, SDA-03, TUC-01, TUC-02, HCC-21, HCC-22, LFB-01, LFB-02, LFB-03, FLO-01, SMT-01, SMT-02, SMT-03, TAN-04. We thank Reserva Natural Serra das Almas (plots SDA-01, SDA-02 and SDA-03) for supporting our research at the reserve. We particularly thank JAXA for providing access free of charge to ALOS-1 PALSAR-1 and ALOS-2 PALSAR-2 data through two research agreements: ER3A2N020 (PI: JMB Carreiras), ER3A2N035 (PI: C Ryan). We also thank the European Space Agency for providing access to ALOS-1 PALSAR-1 data acquired over Africa through their ALOS PALSAR Online Dissemination Service (<https://alos-palsar-ds.eo.esa.int/oads/accessible>). The Alaska Satellite Facility provided access to ALOS-1 PALSAR-1 scenes acquired over Latin America (<https://asf.alaska.edu/data-sets/sar-data-sets/atos-palsar>). We acknowledge Copernicus Climate Change Service for providing access to ERA5-Land hourly data free of charge. ISRIC-World Soil Information provided access free of charge to SoilGrids. Landsat 5 Thematic Mapper data are courtesy of the U.S. Geological Survey. JMBC, PJM, MW and SQ were supported by the NERC National Centre for Earth Observation (NCEO). DMR received fellowship from FAPESP (#2017/17380-1) and PM is supported by FAPESP (#2021/10639-5). TFD, PM and MMES received research productivity fellowship from the Brazilian National Council for Scientific and Technological Development (CNPq) grants 312589/2022-0, 306563/2022-3 and 308623/2021-5 respectively. MMES, JOS, PMSR and RMS are supported by FAPEMIG (APQ-03020-22). Plot vegetation analyses were enabled by the ForestPlots.net Research Project #198 ('Calibrating radar backscatter with forest structure in the dry tropics of Latin America'). ForestPlots.net is a global collaboration and meta-network coordinated from the University of Leeds.

Appendix A. Supplementary data

Supplementary data to this article can be found online at <https://doi.org/10.1016/j.rse.2025.115213>.

Data availability

The authors do not have permission to share data.

References

Ahlstrom, A., Raupach, M.R., Schurgers, G., Smith, B., Arneth, A., Jung, M., Reichstein, M., Canadell, J.G., Friedlingstein, P., Jain, A.K., Kato, E., Poulter, B., Sitch, S., Stocker, B.D., Viovy, N., Wang, Y.P., Wiltshire, A., Zaehle, S., Zeng, N., 2015. The dominant role of semi-arid ecosystems in the trend and variability of the land CO₂ sink. *Science* 348, 895–899.

Antropov, O., Rauste, Y., Hame, T., Praks, J., 2017. Polarimetric ALOS PALSAR time series in mapping biomass of boreal forests. *Remote Sens.* 9.

Araza, A., Bruin, S., Herold, M., Quegan, S., Labrière, N., Rodríguez-Veiga, P., Avitabile, V., Santoro, M., Mitchard, E.T.A., Ryan, C.M., Phillips, O.L., Willcock, S., Verbeek, H., Carreiras, J., Hein, L., Schelhaas, M.J., Pacheco-Pascagaza, A.M., Bispo, P.D., Laurin, G.V., Vieilledent, G., Slik, F., Wijaya, A., Lewis, S.L., Morel, A., Liang, J.J., Sukhdeo, H., Schepaschenko, D., Cavlovic, J., Gilani, H., Lucas, R., 2022. A comprehensive framework for assessing the accuracy and uncertainty of global above-ground biomass maps. *Remote Sens. Environ.* 272, 112917.

Arneth, A., Sitch, S., Pongratz, J., Stocker, B.D., Ciais, P., Poulter, B., Bayer, A.D., Bondeau, A., Calle, L., Chini, L.P., Gasser, T., Fader, M., Friedlingstein, P., Kato, E., Li, W., Lindeskog, M., Nabel, J.E.M.S., Pugh, T.A.M., Robertson, E., Viovy, N., Yue, C., Zaehle, S., 2017. Historical carbon dioxide emissions caused by land-use changes are possibly larger than assumed. *Nat. Geosci.* 10, 79.

Bharadwaj, P.S., Kumar, S., Kushwaha, S.P.S., Bijkar, W., 2015. Polarimetric scattering model for estimation of above ground biomass of multilayer vegetation using ALOS-PALSAR quad-pol data. *Phys. Chem. Earth* 83–84, 187–195.

Brolly, M., Woodhouse, I.H., 2012. A "matchstick model" of microwave backscatter from a forest. *Ecol. Model.* 237, 74–87.

Cassol, H.L.G., Carreiras, J.M.D., Moraes, E.C., Aragao, L.E.O.E.C., Silva, C.V.D., Quegan, S., Shimabukuro, Y.E., 2019. Retrieving secondary Forest aboveground biomass from Polarimetric ALOS-2 PALSAR-2 data in the Brazilian Amazon. *Remote Sens.* 11.

Chave, J., Rejou-Mechain, M., Burquez, A., Chidumayo, E., Colgan, M.S., Delitti, W.B., Duque, A., Eid, T., Fearnside, P.M., Goodman, R.C., Henry, M., Martinez-Yrizar, A., Mugasha, W.A., Muller-Landau, H.C., Mencuccini, M., Nelson, B.W., Ngomanda, A., Nogueira, E.M., Ortiz-Malavassi, E., Pelissier, R., Ploton, P., Ryan, C.M., Salardiaga, J.G., Vieilledent, G., 2014. Improved allometric models to estimate the aboveground biomass of tropical trees. *Glob. Chang. Biol.* 20, 3177–3190.

Chowdhury, T.A., Thiel, C., Schmullius, C., 2014. Growing stock volume estimation from L-band ALOS PALSAR polarimetric coherence in Siberian forest. *Remote Sens. Environ.* 155, 129–144.

Cloude, S.R., 1985. Target decomposition-theorems in radar scattering. *Electron. Lett.* 21, 22–24.

Cloude, S.R., Pottier, E., 1996. A review of target decomposition theorems in radar polarimetry. *IEEE Trans. Geosci. Remote Sens.* 34, 498–518.

Cloude, S.R., Pottier, E., 1997. An entropy based classification scheme for land applications of polarimetric SAR. *IEEE Trans. Geosci. Remote Sens.* 35, 68–78.

Conti, G., Gorné, L.D., Zeballos, S.R., Lipoma, M.L., Gatica, G., Kowaljow, E., Whitworth-Hulse, J.I., Cuchietti, A., Poca, M., Pestoni, S., Fernandes, P.M., 2019. Developing allometric models to predict the individual aboveground biomass of shrubs worldwide. *Glob. Ecol. Biogeogr.* 28, 961–975.

Djoudi, H., Vergles, E., Blackie, R.R., Koame, C.K., Gautier, D., 2015. Dry forests, livelihoods and poverty alleviation: understanding current trends. *Int. For. Rev.* 17, 54–69.

DRYFLOR, Banda-R, K., Delgado-Salinas, A., Dexter, K.G., Linares-Palomino, R., Oliveira-Filho, A., Prado, D., Pullan, M., Quintana, C., Riina, R., Rodríguez, M., Weintritt, J., Acevedo-Rodríguez, P., Adarve, J., Álvarez, E., Aranguren, B., Arteaga, J.C., Aymard, G., Castaño, A., Ceballos-Mago, N., Cogollo, A., Cuadros, H., Delgado, F., Devia, W., Dueñas, H., Fajardo, L., Fernández, A., Fernández, M.A., Franklin, J., Freid, E.H., Galetti, L.A., Gonto, R., González, M.R., Graveson, R., Helmer, E.H., Idárraga, A., López, R., Marcano-Vega, H., Martínez, O.G., Maturó, H.M., McDonald, M., McLaren, K., Melo, O., Mijares, F., Mogni, V., Molina, D., del Moreno, N.P., Nassar, J.M., Neves, D.M., Oakley, L.J., Oatham, M., Olvera-Luna, A., Pezzini, F.F., Dominguez, O.J.R., Ríos, M.E., Rivera, O., Rodríguez, N., Rojas, A., Särkinen, T., Sánchez, R., Smith, M., Vargas, C., Villanueva, B., Pennington, R.T., 2016. Plant diversity patterns in neotropical dry forests and their conservation implications. *Science* 353, 1383–1387. <https://doi.org/10.1126/science.aaf5080>.

Duncanson, L.I., Niemann, K.O., Wulder, M.A., 2010. Estimating forest canopy height and terrain relief from GLAS waveform metrics. *Remote Sens. Environ.* 114, 138–154.

ForestPlots.net, Blundo, C., Carilla, J., Grau, R., Malizia, A., Malizia, L., Osinaga-Acosta, O., Bird, M., Bradford, M., Catchpole, D., Ford, A., Graham, A., Hilbert, D., Kemp, J., Laurance, S., Laurance, W., Ishida, F.Y., Marshall, A., Waite, C., Woell, H., Bastin, J.-F., Bauters, M., Beeckman, H., Boeckx, P., Bogaert, J., Canniere, C.D., de Hauleville, T., Doucet, J.-L., Hardy, O., Hubau, W., Kearsley, E., Verbeek, H., Vleminckx, J., Brewer, S.W., Alarcón, A., Araujo-Murakami, A., Arets, E., Arroyo, L., Chavez, E., Fredericksen, T., Villaruelo, R.G., Sibaute, G.G., Killeen, T., Licona, J.C., Lleigue, J., Mendoza, C., Murakami, S., Gutierrez, A.P., Pardo, G., Peña-Claros, M., Poorter, L., Toledo, M., Mayo, J.V., Viscarra, L.J., Vos, V., Ahumada, J., Almeida, E., Almeida, J., de Oliveira, E.A., da Cruz, W.A., de Oliveira, A.A., Carvalho, Fábricio Alvim, Obermuller, F.A., Andrade, A., Antunes, Carvalho Fernanda, Vieira, S.A., Aquino, A.C., Aragão, L., Aratijo, A.C., Banin, L., Barlow, J., Bennett, A.,

Berenguer, E., Berry, N., Bird, N.M., Blackburn, G.A., Brearley, F., Brienen, R., Burslem, D., Carvalho, L., Cho, P., Coelho, F., Collins, M., Coomes, D., Cuni-Sanchez, A., Dargie, G., Dexter, K., Disney, M., Draper, F., Duan, M., Esquivel-Muelbert, A., Ewers, R., Fadrique, B., Fauset, S., Feldpausch, T.R., França, F., Galbraith, D., Gilpin, M., Gloor, E., Grace, J., Hamer, K., Harris, D., Jeffery, K., Jucker, T., Kalamandeen, M., Klitgaard, B., Levesley, A., Lewis, S.L., Lindsell, J., Lopez-Gonzalez, G., Lovett, J., Malhi, Y., Marthews, T., McIntosh, E., Melgaço, K., Milliken, W., Mitchard, E., Moonlight, P., Moore, S., Morel, A., Peacock, J., Peh, K.S.-H., Pendry, C., Pennington, R.T., de Pereira, L.O., Peres, C., Phillips, O.L., Pickavance, G., Pugh, T., Qie, L., Riutta, T., Roucoux, K., Ryan, C., Sarkinen, T., Valeria, C.S., Spracklen, D., Stas, S., Sullivan, M., Swaine, M., Talbot, J., Taplin, J., Vedovato, L., Willcock, S., Williams, M., Alves, L., Loayza, P.A., Arellano, G., Asa, C., Ashton, P., Asner, G., Brnic, T., Brown, F., Burnham, R., Clark, C., Comiskey, J., Damasco, G., Davies, S., Fiore, T.D., Erwin, T., Farfan-Rios, W., Hall, J., Kenfack, D., Lovejoy, T., Martin, R., Montiel, O.M., Pipoly, J., Pitman, N., Poulsen, J., Primack, R., Silman, M., Steininger, M., Swamy, V., Terborgh, J., Thomas, D., Umunay, P., Uriarte, M., Torre, E.V., Wang, O., Young, K., Hernández, L., Fernández, R.H., Ramírez-Angulo, H., Salcedo, P., Sanjoa, E., Serrano, J., Torres-Lezama, A., Le, T.C., Le, T.T., Tran, H.D., 2021. Taking the pulse of earth's tropical forests using networks of highly distributed plots. *Biol. Conserv.* 260, 108849. <https://doi.org/10.1016/j.biocon.2020.108849>.

Freeman, A., Durden, S.L., 1998. A three-component scattering model for polarimetric SAR data. *IEEE Trans. Geosci. Remote Sens.* 36, 963–973.

Gou, Y.Q., Ryan, C.M., Reiche, J., 2022. Large area aboveground biomass and carbon stock mapping in woodlands in Mozambique with L-band radar: improving accuracy by accounting for soil moisture effects using the water cloud model. *Remote Sens.* 14.

Hastie, T., Tibshirani, R., 1986. Generalized additive models. *Stat. Sci.* 1, 297–310.

Imhoff, M.L., 1995. A theoretical analysis of the effect of forest structure on synthetic aperture radar backscatter and the remote sensing of biomass. *IEEE Trans. Geosci. Remote Sens.* 33, 341–351. <https://doi.org/10.1109/TGRS.1995.8746015>.

Jackson, T.J., Schmugge, T.J., 1991. Vegetation effects on the microwave emission of soils. *Remote Sens. Environ.* 36, 203–212. [https://doi.org/10.1016/0034-4257\(91\)90057-D](https://doi.org/10.1016/0034-4257(91)90057-D).

Kline, R.B., 2016. *Principles and practice of structural equation modeling*, 4th ed. The Guilford Press.

Koyama, C.N., Watanabe, M., Hayashi, M., Ogawa, T., Shimada, M., 2019. Mapping the spatial-temporal variability of tropical forests by ALOS-2 L-band SAR big data analysis. *Remote Sens. Environ.* 233, 111372. <https://doi.org/10.1016/j.rse.2019.111372>.

Le Toan, T., Beaudoin, A., Riou, J., Guyon, D., 1992. Relating forest biomass to Sar data. *IEEE Trans. Geosci. Remote Sens.* 30, 403–411.

Lee, J.-S., Pottier, E., 2009. *Polarimetric Radar Imaging: From Basics to Applications*. CRC Press, Boca Raton.

Lopez-Gonzalez, G., Lewis, S.L., Burkitt, M., Phillips, O.L., 2011. ForestPlots.net: a web application and research tool to manage and analyse tropical forest plot data. *J. Veg. Sci.* 22, 610–613.

Lucas, R.M., Cronin, N., Lee, A., Moghaddam, M., Witte, C., Tickle, P., 2006. Empirical relationships between AIRSAR backscatter and LiDAR-derived forest biomass, Queensland, Australia. *Remote Sens. Environ.* 100, 407–425. <https://doi.org/10.1016/j.rse.2005.10.019>.

Lucas, R., Armston, J., Fairfax, R., Fensham, R., Accad, A., Carreiras, J., Kelley, J., Bunting, P., Clewley, D., Bray, S., Metcalfe, D., Dwyer, J., Bowen, M., Eyre, T., Laidlaw, M., Shimada, M., 2010. An evaluation of the ALOS PALSAR L-band backscatter above ground biomass relationship Queensland, Australia: impacts of surface moisture condition and vegetation structure. *IEEE J. Select. Top. Appl. Earth Observ. Remote Sens.* 3, 576–593.

Mascolo, L., Cloude, S.R., Lopez-Sanchez, J.M., 2022. Model-based decomposition of dual-pol SAR data: application to Sentinel-1. *IEEE Trans. Geosci. Remote Sens.* 60, 1–19. <https://doi.org/10.1109/TGRS.2021.3137588>.

Mattia, F., LeToan, T., Souyris, J.C., DeCarolis, G., Flory, N., Posa, F., Pasquariello, G., 1997. The effect of surface roughness on multifrequency polarimetric SAR data. *IEEE Trans. Geosci. Remote Sens.* 35, 954–966.

McNicol, I.M., Ryan, C.M., Mitchard, E.T.A., 2018. Carbon losses from deforestation and widespread degradation offset by extensive growth in African woodlands. *Nat. Commun.* 9.

McNicol, I.M., Keane, A., Burgess, N.D., Bowers, S.J., Mitchard, E.T.A., Ryan, C.M., 2023. Protected areas reduce deforestation and degradation and enhance woody growth across African woodlands. *Commun. Earth Environ.* 4, 392.

Mermoz, S., Réjou-Méchain, M., Villard, L., Le Loan, T., Rossi, V., Gourlet-Fleury, S., 2015. Decrease of L-band SAR backscatter with biomass of dense forests. *Remote Sens. Environ.* 159, 307–317.

Monteith, A.R., Ulander, L.M.H., 2018. Temporal survey of P- and L-band polarimetric backscatter in boreal forests. *IEEE J. Select. Top. Appl. Earth Observ. Remote Sens.* 11, 3564–3577. <https://doi.org/10.1109/JSTARS.2018.2814825>.

Moonlight, P.W., Banda-R, K., Phillips, O.L., Dexter, K.G., Pennington, R.T., Baker, T.R., Lima, H.C., Fajardo, L., Gonzalez-M, R., Linares-Palomino, R., Lloyd, J., Nascimento, M., Prado, D., Quintana, C., Riña, R., Rodriguez, M.G.M., Villega, D.M., Aquino, A.C.M.M., Arroyo, L., Bezerra, C., Brunello, A.T., Brienen, R.J.W., Cardoso, D., Chao, K.J., Coutinho, I.A.C., Cunha, J., Domingues, T., Santo, M.M.E., Feldpausch, T.R., Fernandes, M.F., Goodwin, Z.A., Jiménez, E.M., Levesley, A., Lopez-Toledo, L., Marimon, B., Miatto, R.C., Mizushima, M., Monteagudo, A., Moura, M.S.B., Murakami, A., Neves, D., Chequín, R.N., Oliveira, T.C.D., Oliveira, E.A., Queiroz, L.P., Pilon, A., Ramos, D.M., Reynel, C., Rodrigues, P.M.S., Santos, R., Särkinen, T., Silva, V.F., Souza, R.M.S., Vasquez, R., Veenendaal, E., 2021. Expanding tropical forest monitoring into dry forests: the DRYFLOR protocol for permanent plots. *Plants People Planet* 3, 295–300.

Munoz-Sabater, J., Dutra, E., Agusti-Panareda, A., Albergel, C., Arduini, G., Balsamo, G., Bousetta, S., Choulga, M., Harrigan, S., Hersbach, H., Martens, B., Miralles, D.G., Piles, M., Rodriguez-Fernandez, N.J., Zsoter, E., Buontempo, C., Thepaut, J.N., 2021. ERA5-land: a state-of-the-art global reanalysis dataset for land applications. *Earth Syst. Sci. Data* 13, 4349–4383.

Palomeque, M., Ferreyra, J., Thibeault, M., 2024. Monitoring results of the SAOCOM-1 constellation: a mission overview and summary of results. In: *IEEE Geoscience and Remote Sensing Magazine*.

Pearl, J., 2012. The causal foundations of structural equation modeling. In: *Handbook of Structural Equation Modeling*. The Guilford Press, New York, NY, US, pp. 68–91.

Pennington, R.T., Lehmann, C.E.R., Rowland, L.M., 2018. Tropical savannas and dry forests. *Curr. Biol.* 28, 541–545.

Piao, S., Huang, M., Liu, Z., Wang, X.H., Ciais, P., Canadell, J.G., Wang, K., Bastos, A., Friedlingstein, P., Houghton, R.A., Le Quere, C., Liu, Y.W., Myneni, R.B., Peng, S.S., Pongratz, J., Sitch, S., Yan, T., Wang, Y.L., Zhu, Z.C., Wu, D.H., Wang, T., 2018. Lower land-use emissions responsible for increased net land carbon sink during the slow warming period. *Nat. Geosci.* 11, 739.

Piao, S.L., Wang, X.H., Wang, K., Li, X.Y., Bastos, A., Canadell, J.G., Ciais, P., Friedlingstein, P., Sitch, S., 2020. Interannual variation of terrestrial carbon cycle: issues and perspectives. *Glob. Chang. Biol.* 26, 300–318. <https://doi.org/10.1111/gcb.12484>.

Poggio, L., Sousa, L.M., Batjes, N.H., Heuvelink, G.B.M., Kempen, B., Ribeiro, E., Rossiter, D., 2021. *SoilGrids 2.0: producing soil information for the globe with quantified spatial uncertainty*. *Soil* 7, 217–240.

Quegan, S., Le Toan, T., Chave, J., Dall, J., Extrayat, J.-F., Minh, D.H.T., Lomas, M., D'Alessandro, M.M., Paillou, P., Papathanassiou, K., Rocca, F., Saatchi, S., Scipal, K., Shugart, H., Smallman, T.L., Soja, M.J., Tebaldo, S., Ulander, L., Villard, L., Williams, M., 2019. The European Space Agency BIOMASS mission: measuring forest above-ground biomass from space. *Remote Sens. Environ.* 227, 44–60. <https://doi.org/10.1016/j.rse.2019.03.032>.

R Core Team, 2023. *R A Language and Environment for Statistical Computing*. R Foundation for Statistical Computing, Vienna [WWW Document]. URL (accessed 7.23.25).

Rejou-Mechain, M., Muller-Landau, H.C., Dett, M., Thomas, S.C., Le Toan, T., Saatchi, S., Barreto-Silva, J.S., Bourg, N.A., Bunyavejchewin, S., Butt, N., Brockelman, W.Y., Cao, M., Cardenas, D., Chiang, J.M., Chuyong, G.B., Clay, K., Condit, R., Dattaraja, H.S., Davies, S.J., Duque, A., Esufali, S., Ewango, C., Fernando, R.H.S., Fletcher, C.D., Gunatilleke, I.A.U.N., Hao, Z., Harms, K.E., Hart, T.B., Heraut, B., Howe, R.W., Hubbell, S.P., Johnson, D.J., Kenfack, D., Larson, A.J., Lin, L., Lin, Y., Lutz, J.A., Makana, J.R., Malhi, Y., Marthews, T.R., McEwan, R.W., McMahon, S.M., McShea, W.J., Muscarella, R., Nathalang, A., Noor, N.S.M., Nyctch, C.J., Oliveira, A.A., Phillips, R.P., Pongattanaranuk, N., Punchi-Manage, R., Salim, R., Schurman, J., Sukumar, R., Suresh, H.S., Suwanvecho, U., Thomas, D.W., Thompson, J., Uriarte, M., Valencia, R., Vicentini, A., Wolf, A.T., Yap, S., Yuan, Z., Zartman, C.E., Zimmerman, J.K., Chave, J., 2014. Local spatial structure of forest biomass and its consequences for remote sensing of carbon stocks. *Biogeosciences* 11, 6827–6840.

Richards, J.A., 2009. *Remote Sensing with Imaging Radar*. Springer, Heidelberg, New York.

Rodriguez-Veiga, P., Carreiras, J., Smallman, T.L., Extrayat, J.F., Ndambiri, J., Mutwiri, F., Nyasaka, D., Quegan, S., Williams, M., Balzter, H., 2020. Carbon stocks and fluxes in Kenyan forests and wooded grasslands derived from earth observation and model-data fusion. *Remote Sens.* 12.

Rosseel, Y., 2012. *Lavaan: an R package for structural equation modeling*. *J. Stat. Softw.* 48, 1–36.

Ryan, C.M., Williams, M., Grace, J., 2011. Above- and belowground carbon stocks in a Miombo woodland landscape of Mozambique. *Biotropica* 43, 423–432.

Ryan, C.M., Hill, T., Woollen, E., Ghee, C., Mitchard, E., Cassells, G., Grace, J., Woodhouse, I.H., Williams, M., 2012. Quantifying small-scale deforestation and forest degradation in African woodlands using radar imagery. *Glob. Chang. Biol.* 18, 243–257.

Schlund, M., Davidson, M.W.J., 2018. Aboveground Forest biomass estimation combining L- and P-band SAR acquisitions. *Remote Sens.* 10, 1151. <https://doi.org/10.3390/rs10071151>.

Shimada, M., Ohtaki, T., 2010. Generating large-scale high-quality SAR mosaic datasets: application to PALSAR data for global monitoring. *IEEE J. Select. Top. Appl. Earth Observ. Remote Sens.* 3, 637–656.

Shimada, M., Itoh, T., Motooka, T., Watanabe, M., Shiraishi, T., Thapa, R., Lucas, R., 2014. New global forest/non-forest maps from ALOS PALSAR data (2007–2010). *Remote Sens. Environ.* 155, 13–31.

Smith-Jonforsen, G., Folkesson, K., Hallberg, B., Ulander, L.M.H., 2007. Effects of forest biomass and stand consolidation on P-band backscatter. *IEEE Geosci. Remote Sens. Lett.* 4, 669–673.

Tanase, M.A., Panciera, R., Lowell, K., Tian, S., Garcia-Martin, A., Walker, J.P., 2013. Sensitivity of L-band radar backscatter to forest biomass in semiarid environments: a comparative analysis of parametric and nonparametric models. *IEEE Trans. Geosci. Remote Sens.* 52, 4671–4685. <https://doi.org/10.1109/TGRS.2013.2283521>.

Tanase, M.A., Panciera, R., Lowell, K., Tian, S., Hacker, J.M., Walker, J.P., 2014. Airborne multi-temporal L-band polarimetric SAR data for biomass estimation in semi-arid forests. *Remote Sens. Environ.* 145, 93–104. <https://doi.org/10.1016/j.rse.2014.01.024>.

The SEOSAW Partnership, T.S.E.O.S.A.W, 2021. A network to understand the changing socio-ecology of the southern African woodlands (SEOSAW): challenges, benefits, and methods. *Plants People Planet* 3, 249–267.

Ulaby, F.T., Moore, R.K., Fung, A.K., 1986. *Microwave Remote Sensing. 2: Radar Remote Sensing and Surface Scattering and Emission Theory*. Artech House, Norwood, MA.

Urbazaev, M., Thiel, C., Mathieu, R., Naidoo, L., Levick, S.R., Smit, I.P.J., Asner, G.P., Schmullius, C., 2015. Assessment of the mapping of fractional woody cover in southern African savannas using multi-temporal and polarimetric ALOS PALSAR L-band images. *Remote Sens. Environ.* 166, 138–153.

van Zyl, J., 1989. Unsupervised classification of scattering behavior using radar polarimetry data. *IEEE Trans. Geosci. Remote Sens.* 27, 36–45.

van Zyl, J., 1993. Application of Cloude's target decomposition theorem to polarimetric imaging radar data. In: *Proc. SPIE*, pp. 184–191.

van Zyl, J., Kim, Y., 2011. *Synthetic Aperture Radar Polarimetry*, 1st ed. Wiley, Hoboken, NJ.

Vinya, R., Malhi, Y., Brown, N.D., Fisher, J.B., Brodribb, T., Aragão, L.E.O.C., 2019. Seasonal changes in plant-water relations influence patterns of leaf display in Miombo woodlands: evidence of water conservative strategies. *Tree Physiol.* 39, 104–112. <https://doi.org/10.1093/treephys/tpy062>.

Wessels, K., Li, X.X., Bouvet, A., Mathieu, R., Main, R., Naidoo, L., Erasmus, B., Asner, G.P., 2023. Quantifying the sensitivity of L-band SAR to a decade of vegetation structure changes in savannas. *Remote Sens. Environ.* 284, 113369.

Wiederkehr, N.C., Gama, F.F., Castro, P.B.N., Bispo, P.D., Balzter, H., Sano, E.E., Liesenberg, V., Santos, J.R., Mura, J.C., 2020. Discriminating Forest successional stages, forest degradation, and land use in Central Amazon using ALOS/PALSAR-2 full-polarimetric data. *Remote Sens.* 12.

Williams, M.L., Mitchell, A.L., Milne, A.K., Danaher, T., Horn, G., 2022. Addressing critical influences on L-band radar backscatter for improved estimates of basal area and change. *Remote Sens. Environ.* 272, 112933.

Woodhouse, I.H., Mitchard, E.T.A., Brolly, M., Maniatis, D., Ryan, C.M., 2012. Radar backscatter is not a “direct measure” of forest biomass. *Nat. Clim. Chang.* 2, 556–557. <https://doi.org/10.1038/nclimate1601>.

Yamaguchi, Y., Moriyama, T., Ishido, M., Yamada, H., 2005. Four-component scattering model for polarimetric SAR image decomposition. *IEEE Trans. Geosci. Remote Sens.* 43, 1699–1706.

Yu, Y.F., Saatchi, S., 2016. Sensitivity of L-band SAR backscatter to aboveground biomass of global forests. *Remote Sens.* 8.